Designing Unimodular Sequence Sets With Good Correlations—Including an Application to MIMO Radar

Hao He, *Student Member, IEEE*, Petre Stoica, *Fellow, IEEE*, and Jian Li, *Fellow, IEEE*

***Abstract*—A multiple-input multiple-output (MIMO) radar system that transmits orthogonal waveforms via its antennas can achieve a greatly increased virtual aperture compared with its phased-array counterpart. This increased virtual aperture enables many of the MIMO radar advantages, including enhanced parameter identifiability and improved resolution. Practical radar requirements such as unit peak-to-average power ratio and range compression dictate that we use MIMO radar waveforms that have constant modulus and good auto- and cross-correlation properties. We present in this paper new computationally efficient cyclic algorithms for MIMO radar waveform synthesis. These algorithms can be used for the design of unimodular MIMO sequences that have very low auto- and cross-correlation sidelobes in a specified lag interval, and of very long sequences that could hardly be handled by other algorithms previously suggested in the literature. A number of examples are provided to demonstrate the performances of the new waveform synthesis algorithms.**

***Index Terms*—Autocorrelation, cross-correlation, MIMO radar, range compression, unimodular sequences, waveform design.**

I. Introduction

UNLIKE a traditional phased-array radar system which only transmits scaled versions of a single waveform, a multiple-input multiple-output (MIMO) radar system transmits via its antennas multiple probing signals that can be chosen at will. Particularly, when transmitting orthogonal waveforms, a MIMO radar system can achieve a greatly increased virtual aperture compared to its phased-array counterpart. This increased virtual aperture enables many of the MIMO radar advantages, such as better detection performance [1], improved parameter identifiability [2], refined resolution [3], and direct applicability of adaptive array techniques [4]. Two recent reviews about MIMO radar systems can be found in [5] (for colocated antennas) and [6] (for widely separated antennas); see also the edited book [7].

Besides orthogonality, good auto- and cross-correlation properties of the transmitted waveforms are also often required such as in range compression applications [8]–[10]. In such a case, good auto-correlation means that a transmitted waveform is nearly uncorrelated with its own time-shifted versions, while good cross-correlation indicates that any one of the transmitted waveforms is nearly uncorrelated with other time-shifted transmitted waveforms. Good correlation properties in the above sense ensure that matched filters at the receiver end can easily extract the signals backscattered from the range bin of interest while attenuating signals backscattered from other range bins. Additionally, practical hardware constraints (amplifiers and A/D converters) require that the synthesized waveforms be unimodular, i.e., constant modulus.

There is an extensive literature about MIMO radar waveform design. In [11] and [12] the covariance matrix of the transmitted waveforms is optimized to achieve a given transmit beampattern, while in [13] the waveforms are designed directly to approximate a given covariance matrix. In [14]–[16], on the other hand, some prior information is assumed known (e.g., the target impulse response) and the waveforms are designed to optimize a statistical criterion (e.g., the mutual information between the target impulse response and the reflected signals). More related to our work, [17] and [18] focus on orthogonal waveform design with good auto- and cross-correlation properties, and [19] aims at reducing the sidelobes of the MIMO radar ambiguity function (i.e., both the range and Doppler resolution are considered). We also note that in the area of multiple access wireless communications, the spreading sequence design basically addresses the same problem of synthesizing waveforms with good auto- and cross-correlation properties (see, e.g., [20]).

Extending the approaches in [9] and [21] and detailing the discussions in [22], we present in this paper several new cyclic algorithms (CA) for unimodular MIMO radar waveform design. More specifically, we design MIMO phase codes that have good correlation properties (from now on, we use "correlation" to denote both auto- and cross-correlation). We first formulate the problem in Section II. In Sections III and IV, we extend the CA-new (CAN) and weighted-CAN (WeCAN) algorithms proposed in [21] to the MIMO case; we will still call them CAN and WeCAN for brevity. Both CAN and WeCAN can be used to design good MIMO sequences; the difference is that CAN considers the correlation for all time lags while WeCAN can

Manuscript received January 30, 2009; accepted May 11, 2009. First published June 12, 2009; current version published October 14, 2009. The associate editor coordinating the review of this manuscript and approving it for publication was Dr. Kainam Thomas Wong. This work was supported in part by the Army Research Office (ARO) under Grant W911NF-07-1-0450, the Office of Naval Research (ONR) under Grants N00014-09-1-0211 and N00014-07-1-0193, the National Science Foundation (NSF) under Grant CCF-0634786, the Swedish Research Council (VR) and the European Research Council (ERC). Opinions, interpretations, conclusions, and recommendations are those of the authors and are not necessarily endorsed by the United States Government.

H. He and J. Li are with the Department of Electrical and Computer Engineering, University of Florida, Gainesville, FL 32611-6130 USA (e-mail: haohe@ufl.edu; li@dsp.ufl.edu).

P. Stoica is with the Department of Information Technology, Uppsala University, Uppsala, Sweden (e-mail: ps@it.uu.se).

Color versions of one or more of the figures in this paper are available online at http://ieeexplore.ieee.org.

Digital Object Identifier 10.1109/TSP.2009.2025108

1053-587X/$26.00 © 2009 IEEE

Authorized licensed use limited to: University of Florida. Downloaded on November 18, 2009 at 14:51 from IEEE Xplore. Restrictions apply.

TABLE I
NOTATIONS

a^*:	the complex conjugate of a scalar a
Re$\{a\}$:	the real part of a scalar a
$\|\mathbf{a}\|$:	the Euclidean norm of a vector $\mathbf{a}$
$\mathbf{A}^*$:	the complex conjugate of a matrix $\mathbf{A}$
$\mathbf{A}^T$:	the transpose of a matrix $\mathbf{A}$
$\mathbf{A}^H$:	the conjugate transpose of a matrix $\mathbf{A}$
tr($\mathbf{A}$):	the trace of a matrix $\mathbf{A}$
$\|\mathbf{A}\|$:	the Frobenius norm of a matrix $\mathbf{A}$
$\mathbf{A} \odot \mathbf{B}$:	the Hadamard product of two matrices $\mathbf{A}$ and $\mathbf{B}$ of the same dimension
δ_n:	the Kronecker delta function: $\delta_n = 1$ if $n = 0$ and $\delta_n = 0$ otherwise
$\mathbf{I}_M$:	the identity matrix of dimension $M \times M$
$f(x) * g(x)$:	the convolution of the functions $f(x)$ and $g(x)$
$\lfloor x \rfloor$:	the biggest integer $\leq x$ (real-valued)
arg(x):	the phase angle (in radians) of x

consider selected lags by imposing weights. In Section V, we present an algorithm named CAD (CA-direct) which is a more direct approach to sequence design than the CA algorithm in [9] (see also [13] and [23]). As will be shown in Section VI, CAN can be used to design very long sequences because of its FFT-based operation, and WeCAN and CAD can be used to design sequences that have very low correlation at certain desired lags.

Notation: We use boldface lowercase and uppercase letters to denote vectors and matrices, respectively. See Table I for other notations used throughout this paper.

II. Problem Formulation

Consider a MIMO radar system with M transmit antennas. Each antenna transmits a phase-coded pulse which is composed of N subpulses and can be written in the baseband as (see, e.g., [24])

$$u_m(t) = \frac{1}{\sqrt{T}} \sum_{n=1}^{N} x_m(n) p\left[\frac{t-(n-1)t_b}{t_b}\right], \quad m = 1, \ldots, M \tag{1}$$

where

$$x_m(n) = e^{j\phi_m(n)}, \quad m = 1, \ldots, M \quad \text{and} \quad n = 1, \ldots, N \tag{2}$$

is the phase code to be designed (it is assumed that the phases $\{\phi_m(n)\}$ can be arbitrary values from $[-\pi, \pi]$), $p(t)$ is the shaping subpulse, e.g., a rectangular pulse with amplitude 1 from time 0 to 1, t_b is the time duration of one subpluse and $T = Nt_b$ is the time duration of the whole pulse. The main waveform design problem for such a system is to synthesize the discrete waveform set $\{x_m(n)\}_{m=1,n=1}^{M,N}$ with desired correlation properties.

The (aperiodic) cross-correlation of $\{x_{m_1}(k)\}_{k=1}^{N}$ and $\{x_{m_2}(k)\}_{k=1}^{N}$ at lag n is defined as

$$r_{m_1m_2}(n) = \sum_{k=n+1}^{N} x_{m_1}(k) x_{m_2}^*(k-n) = r_{m_2m_1}^*(-n) \quad m_1, m_2 = 1, \ldots, M, \quad n = 0, \ldots, N-1. \tag{3}$$

When $m_1 = m_2$, (3) becomes the auto-correlation of $\{x_{m_1}(k)\}_{k=1}^{N}$. We can design MIMO radar waveforms with good correlation properties by minimizing the following criterion:

$$\mathcal{E} = \sum_{m=1}^{M} \sum_{n=-N+1, n\neq 0}^{N-1} |r_{mm}(n)|^2 + \sum_{m_1=1}^{M} \sum_{m_2=1, m_2\neq m_1}^{M} \sum_{n=-N+1}^{N-1} |r_{m_1m_2}(n)|^2. \tag{4}$$

To facilitate the following discussion, denote the matrix of the transmitted waveforms by

$$\mathbf{X} = [\mathbf{x}_1 \quad \mathbf{x}_2 \quad \cdots \quad \mathbf{x}_M]_{N\times M} \tag{5}$$

where

$$\mathbf{x}_m = [x_m(1) \quad x_m(2) \quad \cdots \quad x_m(N)]^T \tag{6}$$

is the waveform transmitted by the m^{th} antenna. The waveform covariance matrices for different time lags are given by

$$\mathbf{R}_n = \begin{bmatrix} r_{11}(n) & r_{12}(n) & \cdots & r_{1M}(n) \\ r_{21}(n) & r_{22}(n) & \cdots & r_{2M}(n) \\ \vdots & & \ddots & \vdots \\ r_{M1}(n) & \cdots & \cdots & r_{MM}(n) \end{bmatrix} \quad n = -N+1, \ldots, 0, \ldots, N-1. \tag{7}$$

By using the following "shifting matrix"

$$\mathbf{J}_n = \begin{bmatrix} \overbrace{0\cdots 01}^{n+1} & & 0 \\ & \ddots & \\ & & 1 \\ 0 & & \end{bmatrix}_{N\times N} = \mathbf{J}_{-n}^T \quad n = 0, \ldots, N-1 \tag{8}$$

the $\mathbf{R}_n$ in (7) can be rewritten as

$$\mathbf{R}_n = (\mathbf{X}^H \mathbf{J}_n \mathbf{X})^T = \mathbf{R}_{-n}^H, \quad n = 0, \ldots, N-1. \tag{9}$$

With the above notation, the criterion in (4) can be written more compactly as

$$\mathcal{E} = \|\mathbf{R}_0 - N\mathbf{I}_M\|^2 + 2\sum_{n=1}^{N-1} \|\mathbf{R}_n\|^2. \tag{10}$$

In some radar applications like synthetic aperture radar (SAR) imaging, the transmitted pulse is relatively long (i.e., N is large) so that the signals backscattered from objects in the near and far range bins overlap significantly (see e.g., [9] and the references therein). In this case, only the waveform correlation properties in a certain lag interval around $n = 0$ are relevant to range resolution and a more proper minimization criterion than (10) is given by

$$\tilde{\mathcal{E}} = \|\mathbf{R}_0 - N\mathbf{I}_M\|^2 + 2\sum_{n=1}^{P-1} \|\mathbf{R}_n\|^2 \tag{11}$$

Authorized licensed use limited to: University of Florida. Downloaded on November 18, 2009 at 14:51 from IEEE Xplore. Restrictions apply.

where $P-1$ is the maximum lag that we are interested in. More specifically, $(P-1)t_b$ [t_b is as defined in (1)] should be chosen no smaller than the maximum round trip delay of signals backscattered from near and far range bins.

In the subsequent sections, we will first consider minimizing correlation metrics related to the criterion $\mathcal{E}$ in (10) and then to the criterion $\tilde{\mathcal{E}}$ in (11). We will show that $\mathcal{E}$ cannot be made very small whereas $\tilde{\mathcal{E}}$ can be made practically zero if P and M are sufficiently small relative to N.

III. CAN

The CAN (CA-new) algorithm is associated with the criterion $\mathcal{E}$ in (10), which can be written as

$$\mathcal{E} = \sum_{n=-(N-1)}^{N-1} \|\mathbf{R}_n - N\mathbf{I}_M\delta_n\|^2. \tag{12}$$

The following Parseval-type equality holds true (the proof is similar to that for the case of $M=1$ in [21]):

$$\sum_{n=-(N-1)}^{N-1} \|\mathbf{R}_n - N\mathbf{I}_M\delta_n\|^2 = \frac{1}{2N}\sum_{p=1}^{2N} \|\mathbf{\Phi}(\omega_p) - N\mathbf{I}_M\|^2 \tag{13}$$

where

$$\mathbf{\Phi}(\omega) \triangleq \sum_{n=-N+1}^{N-1} \mathbf{R}_n e^{-j\omega n} \tag{14}$$

is the spectral density matrix of the vector sequence $[x_1(n) \quad \cdots \quad x_M(n)]^T$ and

$$\omega_p = \frac{2\pi}{2N}p, \quad p = 1, \ldots, 2N. \tag{15}$$

The $\mathbf{\Phi}(\omega)$ defined in (14) can be written in the following "periodogram-like" form (see, e.g., [25]):

$$\mathbf{\Phi}(\omega) = \tilde{\mathbf{y}}(\omega)\tilde{\mathbf{y}}^H(\omega) \tag{16}$$

where

$$\tilde{\mathbf{y}}(\omega) = \sum_{n=1}^{N} \mathbf{y}(n)e^{-j\omega n}, \quad \mathbf{y}(n) = \begin{bmatrix} x_1(n) \\ x_2(n) \\ \vdots \\ x_M(n) \end{bmatrix}. \tag{17}$$

It follows from (13) and (16) that (12) can be rewritten as

$$\mathcal{E} = \frac{1}{2N}\sum_{p=1}^{2N} \left\|\tilde{\mathbf{y}}_p\tilde{\mathbf{y}}_p^H - N\mathbf{I}_M\right\|^2. \quad \left(\tilde{\mathbf{y}}_p \triangleq \tilde{\mathbf{y}}(\omega_p)\right). \tag{18}$$

Remark: The $\mathcal{E}$ in (18) cannot be made very small, even without the unit-modulus constraint on the elements of $\mathbf{X}$, because the rank 1 matrix $\tilde{\mathbf{y}}_p\tilde{\mathbf{y}}_p^H$ cannot approximate well a full rank matrix $N\mathbf{I}$. Another way to understand this problem is to examine, instead, the criterion $\tilde{\mathcal{E}}$ defined in (11) where only $\mathbf{R}_0, \mathbf{R}_1, \ldots, \mathbf{R}_{P-1}$ (which are complex-valued $M \times M$ matrices) are considered. $\mathbf{R}_0$ is Hermitian with all diagonal elements equal to N, so setting $\mathbf{R}_0 = N\mathbf{I}$ leads to $M(M-1)$ (real-valued) equations. $\mathbf{R}_1, \ldots, \mathbf{R}_{P-1}$ do not have any special structure; and thus setting them to zero adds $2M^2$ equations for each of them. Thus, the total number of equations is $K = M(M-1) + (P-1)2M^2$. Compared to this, the number of variables that we can manipulate is $M(N-1)$ (for each of the M waveforms there are $N-1$ free phases, as the initial phase does not matter). Therefore, a basic requirement for good performance is that $K \leq M(N-1)$, which can be simplified to: $P \leq (N+M)/2M$. Put differently, only when $P \leq (N+M)/2M$ is it possible to design unimodular waveforms $\mathbf{X}$ that make $\tilde{\mathcal{E}}$ zero; in other cases $\tilde{\mathcal{E}}$ or $\mathcal{E}$ cannot be made equal to zero. ■

Equation (18) is a quartic (i.e., fourth-order) function of the unknowns $\{x_m(n)\}_{m=1,n=1}^{M,N}$. To get a simpler quadratic criterion function of $\{x_m(n)\}_{m=1,n=1}^{M,N}$, note that

$$\begin{aligned}\mathcal{E} &= \frac{1}{2N}\sum_{p=1}^{2N} \mathrm{tr}\left[(\tilde{\mathbf{y}}_p\tilde{\mathbf{y}}_p^H - N\mathbf{I})(\tilde{\mathbf{y}}_p\tilde{\mathbf{y}}_p^H - N\mathbf{I})^H\right] \\ &= \frac{1}{2N}\sum_{p=1}^{2N}(\|\tilde{\mathbf{y}}_p\|^4 - 2N\|\tilde{\mathbf{y}}_p\|^2 + N^2M) \\ &= 2N\sum_{p=1}^{2N}\left(\left\|\frac{\tilde{\mathbf{y}}_p}{\sqrt{2N}}\right\|^2 - \frac{1}{2}\right)^2 + N^2(M-1).\end{aligned} \tag{19}$$

Instead of minimizing (19) with respect to $\mathbf{X}$, we consider the following minimization problem: see equation (20) at the bottom of the page, where "s.t." stands for "subject to", and $\{\boldsymbol{\alpha}_p\}$ are auxiliary variables. Evidently, if (19) (without the constant term $N^2(M-1)$) can be made equal to zero (or "small") by choosing $\mathbf{X}$, so can (20), and vice versa. Thus, the criterion in (19) and (20) are "almost equivalent" in the sense that their minimization is likely to lead to signals with similar correlation properties, provided that good such properties are achievable (see Appendix B for a discussion on this aspect). Note also that, while we use the original criterion $\mathcal{E}$ in (19) to motivate (20), the latter criterion could have been introduced directly as a correlation metric in its own right.

Remark: It is clear from (19) that $\mathcal{E} \geq N^2(M-1) \triangleq \mathcal{E}_{\mathrm{bound}}$. In general, $\mathcal{E}_{\mathrm{bound}}$ is a loose bound. As an example, $\tilde{\mathcal{E}}$ can be

$$\begin{aligned} \min_{\mathbf{X},\{\boldsymbol{\alpha}_p\}_{p=1}^{2N}} \quad & \sum_{p=1}^{2N}\left\|\frac{1}{\sqrt{2N}}\tilde{\mathbf{y}}_p - \boldsymbol{\alpha}_p\right\|^2 \\ \text{s.t.} \quad & |x_m(n)| = 1, \quad m = 1, \ldots, M \quad \text{and} \quad n = 1, \ldots, N \\ & \|\boldsymbol{\alpha}_p\|^2 = \frac{1}{2}, \quad p = 1, \ldots, 2N \quad (\boldsymbol{\alpha}_p \text{ is } M \times 1) \end{aligned} \tag{20}$$

Authorized licensed use limited to: University of Florida. Downloaded on November 18, 2009 at 14:51 from IEEE Xplore. Restrictions apply.

TABLE II
THE CAN ALGORITHM

Step 0: Initialize $\mathbf{X}$ by a randomly generated $N \times M$ matrix or by some good existing sequences.
Step 1: Fix $\tilde{\mathbf{X}}$ and compute $\mathbf{V}$ according to (23).
Step 2: Fix $\mathbf{V}$ and compute $\tilde{\mathbf{X}}$ according to (25).
Step 3: Repeat Steps 1 and 2 until a pre-specified stop criterion is satisfied, e.g., $\|\mathbf{X}^{(i)} - \mathbf{X}^{(i+1)}\| < 10^{-3}$, where $\mathbf{X}^{(i)}$ is the waveform matrix obtained at the i^{th} iteration.

made zero for $M = 1$ only if $P \leq (N+1)/2$ (see the previous *Remark*); this implies that $\mathcal{E}$ cannot be made zero when $M = 1$, whereas $\mathcal{E}_{\text{bound}} = 0$ when $M = 1$. Thus, $\mathcal{E}_{\text{bound}}$ indicates the difficulty of making $\mathcal{E}$ "small" rather than give a tight performance bound. ■

To solve the minimization problem in (20), define

$$\begin{aligned} \mathbf{a}_p^H &= [\, e^{-j\omega_p} \quad \cdots \quad e^{-j2N\omega_p} \,], \\ \mathbf{A} &= \frac{1}{\sqrt{2N}} [\, \mathbf{a}_1 \quad \cdots \quad \mathbf{a}_{2N} \,], \\ \tilde{\mathbf{X}} &= \begin{bmatrix} \mathbf{X} \\ \mathbf{0} \end{bmatrix}_{2N \times M} \end{aligned} \tag{21}$$

and

$$\mathbf{V} = [\, \boldsymbol{\alpha}_1 \quad \cdots \quad \boldsymbol{\alpha}_{2N} \,]^T.$$

Then it is not difficult to observe that

$$\sum_{p=1}^{2N} \left\| \frac{1}{\sqrt{2N}} \tilde{\mathbf{y}}_p - \boldsymbol{\alpha}_p \right\|^2 = \|\mathbf{A}^H \tilde{\mathbf{X}} - \mathbf{V}\|^2 = \|\tilde{\mathbf{X}} - \mathbf{A}\mathbf{V}\|^2. \tag{22}$$

(The second equality in (22) follows from the fact that $\mathbf{A}$ is unitary.) The criterion in (22) can be minimized by means of two iterative (cyclic) steps. For given $\tilde{\mathbf{X}}$ (i.e., $\mathbf{X}$ is given), the minimizer $\{\boldsymbol{\alpha}_p\}_{p=1}^{2N}$ of (22) is given by

$$\boldsymbol{\alpha}_p = \frac{1}{\sqrt{2}} \frac{\mathbf{c}_p}{\|\mathbf{c}_p\|}, \quad p = 1, \ldots, 2N \tag{23}$$

where

$$\mathbf{c}_p^T = \text{the } p^{\text{th}} \text{ row of } (\mathbf{A}^H \tilde{\mathbf{X}}). \tag{24}$$

For given $\mathbf{V}$ (i.e., $\{\boldsymbol{\alpha}_p\}_{p=1}^{2N}$ are given), the minimizer $\{x_m(n)\}$ of (22) is given by

$$x_m(n) = \exp(j \arg(d_{nm})), \;\; m = 1, \ldots, M \text{ and } n = 1, \ldots, N \tag{25}$$

where

$$d_{nm} = \text{the } (n,m)^{\text{th}} \text{ element of } (\mathbf{A}\mathbf{V}). \tag{26}$$

The CAN algorithm thus obtained is summarized in Table II.

Note that the $\mathbf{A}^H \tilde{\mathbf{X}}$ in (24) is the FFT of each column of $\tilde{\mathbf{X}}$ and that the $\mathbf{A}\mathbf{V}$ in (26) is the IFFT of each column of $\mathbf{V}$. Because of these (I)FFT-based computations, the CAN algorithm is quite fast. Indeed, it can be used to design very long sequences, e.g., sequences with $N \sim 10^5$ and $M \sim 10$, which can hardly be handled by other algorithms suggested in the previous literature.

As explained in the *Remarks* in this section, the criterion $\mathcal{E}$ defined in (10) is lower bounded by $N^2(M-1)$ and therefore it cannot be made equal to a "small" value. This unveils the fact that it is not possible to design a set of sequences which are orthogonal to each other and for which all time-shifted correlations are zero. Fortunately, in some application it is desired to minimize the correlations only within a certain time lag interval [e.g., to minimize the $\tilde{\mathcal{E}}$ defined in (11)] and, provided that this interval is not too large [see the *Remark* following (18)], it is possible to make these correlations very small. The WeCAN algorithm presented in the next section is derived to achieve such a goal by introducing different weights for different correlation lags.

IV. WECAN

The WeCAN (weighted-CAN) algorithm aims at minimizing the following criterion:

$$\hat{\mathcal{E}} = \gamma_0^2 \|\mathbf{R}_0 - N\mathbf{I}_M\|^2 + 2 \sum_{n=1}^{N-1} \gamma_n^2 \|\mathbf{R}_n\|^2 \tag{27}$$

where $\{\gamma_n\}_{n=0}^{N-1}$ are real-valued weights. For instance, if we choose $\gamma_n = 1$ for $n = 0, \ldots, P-1$ and $\gamma_n = 0$ otherwise, $\hat{\mathcal{E}}$ becomes the $\tilde{\mathcal{E}}$ defined in (11).

Similarly to the proof of (13), we can show that

$$\hat{\mathcal{E}} = \frac{1}{2N} \sum_{p=1}^{2N} \left\| \tilde{\boldsymbol{\Phi}}(\omega_p) - \gamma_0 N \mathbf{I}_M \right\|^2 \tag{28}$$

where $\{\omega_p\}_{p=1}^{2N}$ is given by (15) and

$$\tilde{\boldsymbol{\Phi}}(\omega) \triangleq \sum_{n=-(N-1)}^{N-1} \gamma_n \mathbf{R}_n e^{-j\omega n} \tag{29}$$

and where $\gamma_n = \gamma_{-n}$ for $n = 1, \ldots, N-1$. To facilitate later developments, γ_0 is chosen such that the matrix

$$\boldsymbol{\Gamma} = \begin{bmatrix} \gamma_0 & \gamma_1 & \cdots & \gamma_{N-1} \\ \gamma_1 & \gamma_0 & \ddots & \vdots \\ \vdots & \ddots & \ddots & \gamma_1 \\ \gamma_{N-1} & \cdots & \gamma_1 & \gamma_0 \end{bmatrix} \tag{30}$$

is positive semi-definite (denoted as $\boldsymbol{\Gamma} \geq 0$). ($\gamma_0$ can be determined in the following way. Let $\tilde{\boldsymbol{\Gamma}}$ be the matrix $\boldsymbol{\Gamma}$ with all diagonal elements set to 0, and let $\lambda_{\min}$ denote the minimum eigenvalue of $\tilde{\boldsymbol{\Gamma}}$; then $\boldsymbol{\Gamma} \geq 0$ if and only if $\gamma_0 + \lambda_{\min} \geq 0$, a condition that can always be satisfied by selecting γ_0.) The condition $\boldsymbol{\Gamma} \geq 0$ is necessary because the matrix square root of $\boldsymbol{\Gamma}$ is needed later on [see (34)].

Authorized licensed use limited to: University of Florida. Downloaded on November 18, 2009 at 14:51 from IEEE Xplore. Restrictions apply.

Similarly to (16), it can be shown that (the proof is similar to that in [21] for the case of $M = 1$):

$$\tilde{\mathbf{\Phi}}(\omega) = \mathbf{Z}^T(\omega)\mathbf{\Gamma}\mathbf{Z}^*(\omega) \tag{31}$$

where

$$\mathbf{Z}^T(\omega) = [\,\mathbf{y}(1)e^{-j\omega} \quad \cdots \quad \mathbf{y}(N)e^{-j\omega N}\,]_{M\times N}. \tag{32}$$

By combining (28) and (31), the criterion function becomes

$$\hat{\mathcal{E}} = \frac{1}{2N}\sum_{p=1}^{2N}\left\|\mathbf{Z}_p^H\mathbf{\Gamma}\mathbf{Z}_p - \gamma_0 N\mathbf{I}_M\right\|^2 \quad (\mathbf{Z}_p \triangleq \mathbf{Z}(\omega_p)). \tag{33}$$

Instead of minimizing (33) with respect to $\mathbf{X}$, we consider the following minimization problem [see the discussion following (20)]:

$$\begin{aligned}\min_{\mathbf{X},\mathbf{U}} \quad & \sum_{p=1}^{2N}\left\|\mathbf{C}\mathbf{Z}_p - \sqrt{\gamma_0 N}\mathbf{U}_p\right\|^2, \\ \text{s.t.} \quad & |x_m(n)| = 1, \quad m = 1,\ldots,M \quad \text{and} \quad n = 1,\ldots,N, \\ & \mathbf{U}_p^H\mathbf{U}_p = \mathbf{I}, \quad p = 1,\ldots,2N, \quad (\mathbf{U}_p \text{ is } N\times M)\end{aligned} \tag{34}$$

where the $N \times N$ matrix $\mathbf{C}$ is a square root of $\mathbf{\Gamma}$ (i.e., $\mathbf{C}^H\mathbf{C} = \mathbf{\Gamma}$).

The minimization problem in (34) can be solved in a cyclic way as follows. For given $\{\mathbf{Z}_p\}_{p=1}^{2N}$ (i.e., $\mathbf{X}$ is given), (34) decouples into $2N$ independent problems, each of which can be written as

$$\begin{aligned}\left\|\mathbf{C}\mathbf{Z}_p - \sqrt{\gamma_0 N}\mathbf{U}_p\right\|^2 = & \ \text{const} \\ -2\text{Re}\left\{\text{tr}\left[\sqrt{\gamma_0 N}\mathbf{U}_p\mathbf{Z}_p^H\mathbf{C}^H\right]\right\}, & \quad p = 1,\ldots,2N\end{aligned} \tag{35}$$

where "const" denotes a term that is independent of the variable $\mathbf{U}_p$. Let

$$\mathbf{Z}_p^H\mathbf{C}^H = \mathbf{U}_1\mathbf{\Sigma}\mathbf{U}_2^H \tag{36}$$

denote the singular value decomposition (SVD) of $\mathbf{Z}_p^H\mathbf{C}^H$, where $\mathbf{U}_1$ is $M \times M$, $\mathbf{\Sigma}$ is $M \times M$ and $\mathbf{U}_2$ is $N \times M$. Then the minimizer $\mathbf{U}_p$ of (35), for fixed $\mathbf{Z}_p$, is given by (see, e.g., [13] and [26]):

$$\mathbf{U}_p = \mathbf{U}_2\mathbf{U}_1^H. \tag{37}$$

Note that the computation of $\{\mathbf{C}\mathbf{Z}_p\}_{p=1}^{2N}$ can be done by means of the FFT. To see this, let

$$\tilde{\mathbf{X}}_m = \mathbf{C}^T \odot [\,\mathbf{x}_m \quad \mathbf{x}_m \quad \cdots \quad \mathbf{x}_m\,]_{N\times N}, \quad m = 1,\ldots,M \tag{38}$$

and

$$\mathbf{F} = \sqrt{2N}\mathbf{A}^H\tilde{\mathbf{F}}, \ \tilde{\mathbf{F}} = \begin{bmatrix}\tilde{\mathbf{X}}_1 & \cdots & \tilde{\mathbf{X}}_M \\ \mathbf{0}_{N\times N} & \cdots & \mathbf{0}_{N\times N}\end{bmatrix}_{2N\times NM} \tag{39}$$

where $\mathbf{A}$ has been defined in (21). Then it is not difficult to observe that the $N \times M$ matrix $\mathbf{C}\mathbf{Z}_p$ is given by reshaping the $NM \times 1$ vector $\mathbf{f}_p$ into each column (from left to right) of $\mathbf{C}\mathbf{Z}_p$, where $\mathbf{f}_p^T$ denotes the p^{th} row of $\mathbf{F}$.

TABLE III
THE WECAN ALGORITHM

Step 0: Initialize $\mathbf{X}$ and select the desired weights $\{\gamma_n\}_{n=0}^{N-1}$ such that the matrix $\mathbf{\Gamma}$ in (30) is positive semi-definite.
Step 1: Fix $\{\mathbf{Z}_p\}_{p=1}^{2N}$ (i.e., $\mathbf{X}$ is given) and compute $\{\mathbf{U}_p\}_{p=1}^{2N}$ according to (37).
Step 2: Fix $\{\mathbf{U}_p\}_{p=1}^{2N}$ and compute $\mathbf{X}$ according to (43).
Step 3: Repeat Steps 1 and 2 until a pre-specified stop criterion is satisfied, e.g., $\|\mathbf{X}^{(i)} - \mathbf{X}^{(i+1)}\| < \epsilon$, where $\mathbf{X}^{(i)}$ is the waveform matrix obtained at the i^{th} iteration. (See the *Remark* in Section VI-D for a brief discussion about how to choose the value of ϵ.)

For given $\{\mathbf{U}_p\}_{p=1}^{2N}$, the minimization problem in (34) also has a closed-form solution with respect to $\mathbf{X}$. Let

$$\mathbf{G}_{2N\times NM} = [\,\mathbf{g}_1 \quad \mathbf{g}_2 \quad \cdots \quad \mathbf{g}_{2N}\,]^T \tag{40}$$

where $\mathbf{g}_p$ denotes the $NM \times 1$ vector given by the columns of $\sqrt{\gamma_0 N}\mathbf{U}_p$ stacked on top of each other. Then the criterion in (34) can be written as equation

$$\begin{aligned}\sum_{p=1}^{2N}\left\|\mathbf{C}\mathbf{Z}_p - \sqrt{\gamma_0 N}\mathbf{U}_p\right\|^2 &= \left\|\sqrt{2N}\mathbf{A}^H\tilde{\mathbf{F}} - \mathbf{G}\right\|^2 \\ &= 2N\left\|\tilde{\mathbf{F}} - \frac{1}{\sqrt{2N}}\mathbf{A}\mathbf{G}\right\|^2.\end{aligned} \tag{41}$$

Equation (41) can be minimized with respect to each element of $\{x_m(n)\}_{m=1,n=1}^{M,N}$ separately. Let x denote a generic element of $\{x_m(n)\}$. Then the corresponding problem is to minimize the following criterion with respect to x:

$$\sum_{k=1}^{N}|\mu_k x - \nu_k|^2 = \text{const} - 2\,\text{Re}\left[\left(\sum_{k=1}^{N}\mu_k^*\nu_k\right)x^*\right] \tag{42}$$

where $\{\mu_k\}_{k=1}^N$ are given by the elements of $\tilde{\mathbf{F}}$ which contain x, and $\{\nu_k\}_{k=1}^N$ are given by the elements of $1/\sqrt{2N}\mathbf{A}\mathbf{G}$ whose positions are the same as those of $\{\mu_k\}_{k=1}^N$ in $\tilde{\mathbf{F}}$. (More specifically, for $k = 1,\ldots,N$, μ_k is given by the $(k,n)^{\text{th}}$ element of $\mathbf{C}$ and ν_k is given by the $(n,(m-1)N+k)^{\text{th}}$ element of $1/\sqrt{2N}\mathbf{A}\mathbf{G}$.) Under the unimodular constraint, the minimizer x of the criterion in (42) is given by

$$x = e^{j\phi}, \quad \phi = \arg\left(\sum_{k=1}^{N}\mu_k^*\nu_k\right). \tag{43}$$

The WeCAN algorithm follows naturally from the above discussions and it is summarized in Table III.

Like CAN, the WeCAN algorithm also makes use of (I)FFT operations (see the $\mathbf{A}^H\tilde{\mathbf{F}}$ in (39) and $\mathbf{A}\mathbf{G}$ in (41)). However, compared to CAN, which needs $2M$ computations of $2N$-point (I)FFT's in one iteration, WeCAN requires $2MN$ computations of $2N$-point (I)FFT's. Moreover, WeCAN requires $2N$ computations of the SVD of an $M \times N$ matrix [see (36)]. Thus, WeCAN is not so computationally efficient as CAN, but it can still be used for relatively large values of N and M, up to $N \sim 10^3$ and $M \sim 10$.

Authorized licensed use limited to: University of Florida. Downloaded on November 18, 2009 at 14:51 from IEEE Xplore. Restrictions apply.

V. CAD

The CAD (CA-direct) algorithm aims at minimizing a particular form of the criterion $\hat{\mathcal{E}}$ in (27):

$$\hat{\mathcal{E}}_{\mathrm{CAD}} = P\|\mathbf{R}_0 - N\mathbf{I}_M\|^2 + 2\sum_{n=1}^{P-1}(P-n)\|\mathbf{R}_n\|^2 \qquad (44)$$

which can be obtained from (27) by choosing weights $\gamma_n^2 = P-n$ for $n=0,\ldots,P-1$ and $\gamma_n^2=0$ otherwise. The above choice of $\{\gamma_n\}_{n=0}^{N-1}$ results from the following problem formulation that is simple and direct. Consider the following matrix:

$$\bar{\mathbf{X}} = [\,\bar{\mathbf{X}}_1 \quad \cdots \quad \bar{\mathbf{X}}_M\,]_{(N+P-1)\times MP} \qquad (45)$$

where

$$\bar{\mathbf{X}}_m = \begin{bmatrix} x_m(1) & & \\ \vdots & \ddots & \\ \vdots & & x_m(1) \\ x_m(N) & & \vdots \\ & \ddots & \vdots \\ & & x_m(N) \end{bmatrix}_{(N+P-1)\times P} \qquad m=1,\ldots,M. \qquad (46)$$

Then it is easy to observe that the $\hat{\mathcal{E}}_{\mathrm{CAD}}$ defined in (44) can be expressed as

$$\hat{\mathcal{E}}_{\mathrm{CAD}} = \left\|\bar{\mathbf{X}}^H\bar{\mathbf{X}} - N\mathbf{I}_{MP}\right\|^2. \qquad (47)$$

Remark: The papers [9], [13], and [21] have considered the following problem, instead of minimizing (47):

$$\begin{aligned} \min_{\mathbf{X},\mathbf{U}} \quad & \|\bar{\mathbf{X}} - \sqrt{N}\mathbf{U}\|^2, \\ \text{s.t.} \quad & |x_m(n)| = 1, \quad m=1,\ldots,M \quad \text{and} \quad n=1,\ldots,N, \\ & \mathbf{U}^H\mathbf{U} = \mathbf{I}, \quad (\mathbf{U}\,\text{is}\,(N+P-1)\times MP) \end{aligned} \qquad (48)$$

and the cyclic algorithm corresponding to (48) was named CA; see Section VI for some examples that involve CA. ■

Next we show how to minimize (47) with respect to a generic waveform element $x_m(n) = e^{j\phi_{mn}}$. Let $\tilde{\bar{\mathbf{X}}}_{mn}$ denote the matrix $\bar{\mathbf{X}}$ with all elements comprising $x_m(n)$ set to 0 ($x_m(n)$ appears P times in $\bar{\mathbf{X}}$), and let $\bar{\mathbf{I}}_{mn}$ denote an $(N+P-1)\times MP$ matrix whose elements are all 0 except those elements whose positions are the same as the positions of $x_m(n)$ in $\bar{\mathbf{X}}$, which are 1. Then we have

$$\begin{aligned} \bar{\mathbf{X}}^H\bar{\mathbf{X}} &= (\tilde{\bar{\mathbf{X}}}_{mn} + e^{j\phi_{mn}}\bar{\mathbf{I}}_{mn})^H(\tilde{\bar{\mathbf{X}}}_{mn} + e^{j\phi_{mn}}\bar{\mathbf{I}}_{mn}) \\ &= \tilde{\bar{\mathbf{X}}}_{mn}^H\tilde{\bar{\mathbf{X}}}_{mn} + e^{j\phi_{mn}}\tilde{\bar{\mathbf{X}}}_{mn}^H\bar{\mathbf{I}}_{mn} + e^{-j\phi_{mn}}\bar{\mathbf{I}}_{mn}^H\tilde{\bar{\mathbf{X}}}_{mn} \\ &\quad + \bar{\mathbf{I}}_{mn}^H\bar{\mathbf{I}}_{mn}. \end{aligned} \qquad (49)$$

TABLE IV
THE CAD ALGORITHM

Step 0: Initialize $\bar{\mathbf{X}}$ in (45).
Step 1: Minimize the criterion in (47) with respect to $x_1(1)$ (by solving the generic problem in (53)), then with respect to $x_1(2)$, ..., and so on up to $x_M(N)$.
Step 2: Repeat Step 1 until a pre-specified stop criterion is satisfied (see the last step of the WeCAN algorithm in Table III).

Thus, the criterion in (47) can be written as (below the dependence of $\tilde{\bar{\mathbf{X}}}_{mn}$, $\bar{\mathbf{I}}_{mn}$ and ϕ_{mn} on m and n is omitted for brevity)

$$\begin{aligned} &\left\|\bar{\mathbf{X}}^H\bar{\mathbf{X}} - N\mathbf{I}\right\|^2 \\ &= \left\| e^{j\phi}\tilde{\bar{\mathbf{X}}}^H\bar{\mathbf{I}} + e^{-j\phi}\bar{\mathbf{I}}^H\tilde{\bar{\mathbf{X}}} \right. \\ &\qquad \left. -\left(N\mathbf{I} - \tilde{\bar{\mathbf{X}}}^H\tilde{\bar{\mathbf{X}}} - \bar{\mathbf{I}}^H\bar{\mathbf{I}}\right)\right\|^2 \\ &= \mathrm{tr}\Big[(e^{j\phi}\tilde{\bar{\mathbf{X}}}^H\bar{\mathbf{I}} + e^{-j\phi}\bar{\mathbf{I}}^H\tilde{\bar{\mathbf{X}}} - \bar{\mathbf{S}})^H \\ &\qquad \times(e^{j\phi}\tilde{\bar{\mathbf{X}}}^H\bar{\mathbf{I}} + e^{-j\phi}\bar{\mathbf{I}}^H\tilde{\bar{\mathbf{X}}} - \bar{\mathbf{S}})\Big] \\ &= \mathrm{const} - 4\,\mathrm{Re}\Big[e^{j\phi}\mathrm{tr}(\tilde{\bar{\mathbf{X}}}^H\bar{\mathbf{I}}\bar{\mathbf{S}})\Big] \\ &\qquad +2\,\mathrm{Re}\Big[e^{2j\phi}\mathrm{tr}(\tilde{\bar{\mathbf{X}}}^H\bar{\mathbf{I}}\tilde{\bar{\mathbf{X}}}^H\bar{\mathbf{I}})\Big] \end{aligned} \qquad (50)$$

where $\bar{\mathbf{S}} = N\mathbf{I} - \tilde{\bar{\mathbf{X}}}^H\tilde{\bar{\mathbf{X}}} - \bar{\mathbf{I}}^H\bar{\mathbf{I}}$ and "const" denotes a term that is independent of the variable ϕ. To write (50) more compactly, we let

$$\begin{aligned} \mathrm{tr}(\tilde{\bar{\mathbf{X}}}^H\bar{\mathbf{I}}\bar{\mathbf{S}}) &= a_1e^{j\theta_1}, \quad (a_1 \ge 0) \\ \mathrm{tr}(\tilde{\bar{\mathbf{X}}}^H\bar{\mathbf{I}}\tilde{\bar{\mathbf{X}}}^H\bar{\mathbf{I}}) &= a_2e^{j\theta_2} \quad (a_2 \ge 0) \end{aligned} \qquad (51)$$

which leads to

$$\begin{aligned} &\left\|\bar{\mathbf{X}}^H\bar{\mathbf{X}} - N\mathbf{I}\right\|^2 \\ &\quad = \mathrm{const} - 4\ \mathrm{Re}\left[e^{j\phi}a_1e^{j\theta_1}\right] + 2\ \mathrm{Re}\left[e^{2j\phi}a_2e^{j\theta_2}\right] \\ &\quad = \mathrm{const} - 4a_1\cos(\phi+\theta_1) + 2a_2\cos(2\phi+\theta_2). \end{aligned} \qquad (52)$$

The discussion above shows that the minimization of (47) with respect to a single waveform element $x_m(n) = e^{j\phi_{mn}}$ is equivalent to the following problem:

$$\min_{-\pi\le\phi\le\pi} -2a_1\cos(\phi+\theta_1) + a_2\cos(2\phi+\theta_2) \qquad (53)$$

which can be easily solved numerically (see Appendix A). Then we propose that (47) be minimized with respect to each $\{x_m(n)\}_{m,n=1}^{M,N}$ in a one by one manner, and the process be repeated iteratively. The resulting algorithm is called CAD (CA-direct) and is summarized in Table IV. (The adjective "direct" attached to the name of this algorithm is motivated by the fact that the algorithm deals directly with the criterion in (44), and not with the related one in (48).)

Authorized licensed use limited to: University of Florida. Downloaded on November 18, 2009 at 14:51 from IEEE Xplore. Restrictions apply.

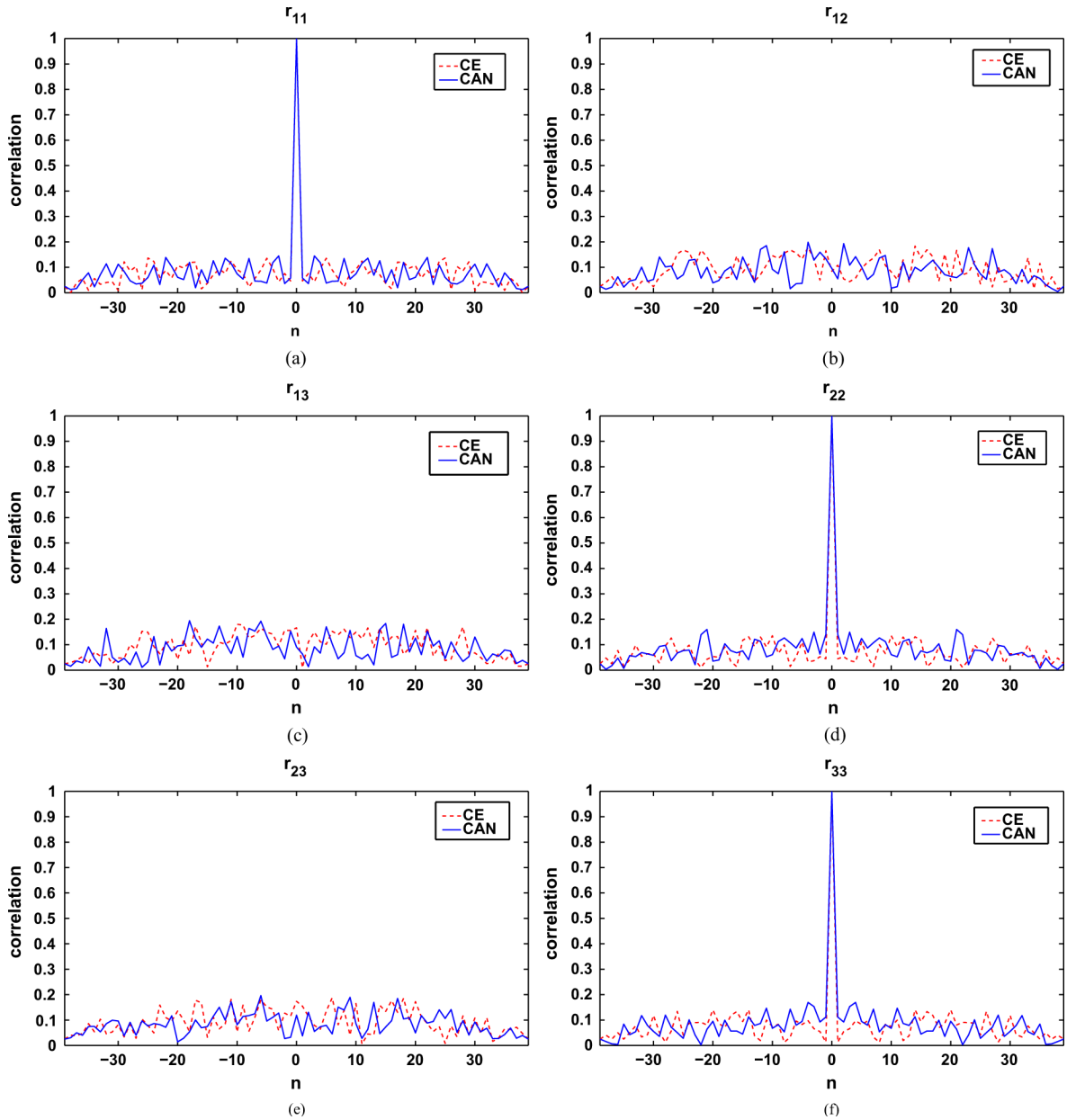

Fig. 1. Correlations of the 40-by-3 CE and CAN sequences.

VI. Numerical Examples

A. The Minimization of $\mathcal{E}$ in (10)

Consider minimizing the criterion $\mathcal{E}$ in (10), i.e., minimizing all correlation sidelobes: $r_{mm}(n)$ for all m and $n \neq 0$, and $r_{m_1m_2}(n)$ for all $m_1 \neq m_2$ and n. Suppose that the number of transmit antennas is $M = 3$ and the number of samples is $N = 40$. We compare the CAN sequence with the CE (cross entropy) sequence in [18]. (From here on, "sequence" will be short for "an N-by-M set of sequences".) We use a randomly generated sequence to initialize CAN (see Step 0 in Table II). 100 Monte Carlo trials are run (i.e., 100 random initializations) and the sequence with the lowest correlation sidelobe peak is kept. The 40-by-3 CE sequence is given in Table I of [18].

Fig. 1 shows the correlations ($r_{11}, r_{12}, \ldots, r_{33}$, normalized by N) of the CAN sequence and CE sequence. The CE sequence is slightly better than the CAN sequence in terms of correlation sidelobe peaks. However, our goal is to minimize $\mathcal{E}$ or equivalently the following normalized fitting error:

$$\mathcal{E}_{\text{norm}} = \frac{\mathcal{E}}{MN^2} = \left(\|\mathbf{R}_0 - N\mathbf{I}\|^2 + 2\sum_{n=1}^{N-1} \|\mathbf{R}_n\|^2 \right) / (MN^2). \tag{54}$$

The CAN sequence gives a fitting error of 2.00, whereas the CE sequence has a bigger fitting error equal to 2.23.

Note that although the CAN and CE sequences show comparable performances (also comparable to the performance of other sequences like the ones in [17]), the CAN algorithm works much faster than other existing algorithms, because CAN is based on FFT computations. For the above parameter set ($N = 40$ and $M = 3$), the CAN algorithm consumes less than one second on an ordinary PC to complete one Monte Carlo trial.

Authorized licensed use limited to: University of Florida. Downloaded on November 18, 2009 at 14:51 from IEEE Xplore. Restrictions apply.

The overall computation time is still short if we run plenty of Monte Carlo trials and pick up the best sequence. Moreover, the computation time of CAN grows roughly as $O(MN\log N)$ so that CAN can handle very large values of N, up to $N\sim 10^5$. In contrast, the cross entropy [18] or simulated annealing based methods [17] are relatively involved and become impractical for large values of N. In fact, we were unable to find in the literature any MIMO code that is designed for good (aperiodic) correlations and at the same time is sufficiently long to be comparable with the CAN sequence.

For relatively large values of N, we decided to employ the Hadamard sequence (see, e.g., [27]), which is easy to generate (for virtually any length that is a power of 2) and is frequently used in wireless communications, for comparison. We also scrambled the Hadamard sequence with a PN (pseudo-noise) sequence to lower its correlation sidelobes. We compare the CAN sequence (100 Monte Carlo trials are run for each N and the result with the lowest correlation sidelobe peak is shown) and the QPSK Hadamard+PN sequence for $M=3$ and $N=2^7,\ldots,2^{13}$. Fig. 2 compares the sequences in terms of three criteria: the auto-correlation sidelobe peak, the cross-correlation peak and the normalized fitting error [defined in (54)]. The CAN sequence outperforms the Hadamard + PN sequence with respect to each criterion. In fact, the advantage of the CAN algorithm lies not only in the significant length and the low correlation sidelobes of the designed sequences, but also in the easy generation (using different initial conditions) of many sequences which are of the same N-by-M dimension and all have reasonably low correlation sidelobes. These randomly distributed waveform sets are useful to some application areas, like to countering the coherent repeater jamming in radar systems (see, e.g., [8] and [17]).

Remark: In the derivation of the CAN algorithm (as well as those of the WeCAN and CAD algorithms), we have assumed that the phases $[\{\phi_m(n)\}_{m=1,n=1}^{M,N}$, see (2)] can take on arbitrary values from $-\pi$ to π. Interestingly, if we quantize the phases, the performance of the designed sequences will not degrade significantly if the quantization is not too rough. See Appendix C for an example. ■

B. The Minimization of $\tilde{\mathcal{E}}$ in (11)

Consider minimizing the criterion $\tilde{\mathcal{E}}$ in (11), i.e., minimizing the correlation sidelobes for lags not larger than $P-1$: $r_{mm}(n)$ for all m and $1\le n\le P-1$, and $r_{m_1m_2}(n)$ for all $m_1\ne m_2$ and $0\le n\le P-1$. Suppose that the number of transmit antennas is $M=4$, the number of samples is $N=256$ and the number of correlation lags we want to consider is $P=50$. Similarly to (54), the normalized fitting error for this scenario is defined as

$$\tilde{\mathcal{E}}_{\rm norm}=\frac{\tilde{\mathcal{E}}}{MN^2}=\left(\|\mathbf{R}_0-N\mathbf{I}\|^2+2\sum_{n=1}^{P-1}\|\mathbf{R}_n\|^2\right)/(MN^2). \tag{55}$$

We also define the correlation level as

$$\text{correlation level}=20\log_{10}\frac{\|\mathbf{R}_n-N\mathbf{I}\delta_n\|}{\sqrt{MN^2}},\quad n=-N+1,\ldots,0,\ldots,N-1 \tag{56}$$

which measures the "total" correlation for a certain lag.

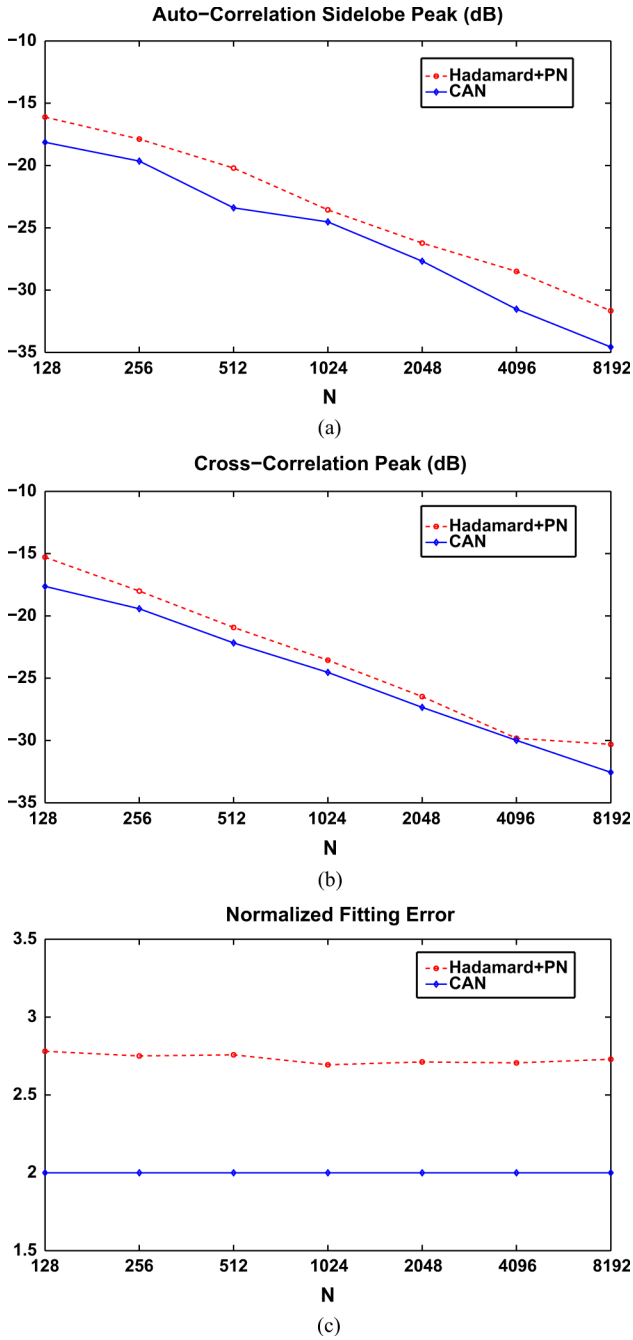

Fig. 2. Comparison between the CAN sequence and the Hadamard + PN sequence with $M=3$ and $N=2^7,\ldots,2^{13}$ in terms of (a) the auto-correlation sidelobe peak, (b) the cross-correlation peak, and (c) the normalized fitting error as defined in (54).

We compare the WeCAN algorithm and the previously suggested CA algorithm (see (48) and also [9] and [13]). We use a randomly generated unimodular sequence to initialize both WeCAN and CA. To construct the matrix $\mathbf{\Gamma}$ in (30) that is needed in WeCAN, we choose

$$\gamma_n^2=\begin{cases}1, & n\in[1,P-1]\\ 0, & n\in[P,N-1]\end{cases} \tag{57}$$

and γ_0 is chosen to ensure that $\mathbf{\Gamma}\ge 0$ [more exactly we choose $\gamma_0=25.5$ following the discussion right after (30)].

Authorized licensed use limited to: University of Florida. Downloaded on November 18, 2009 at 14:51 from IEEE Xplore. Restrictions apply.

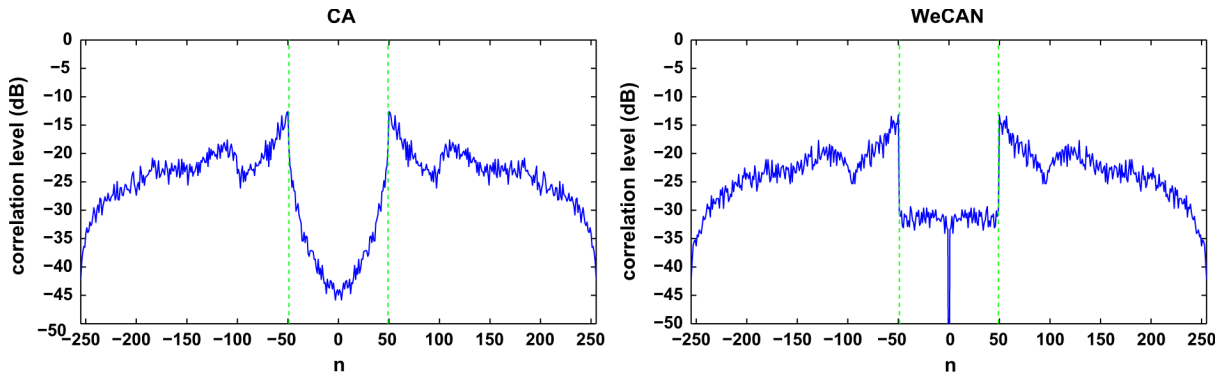

Fig. 3. Correlation levels of the CA sequence and the WeCAN sequence for $N = 256$, $M = 4$ and $P = 50$. (The dotted vertical lines signify the boundary of the time lag interval under consideration.) (a) The CA sequence and (b) the WeCAN sequence.

TABLE V
COMPARISON BETWEEN CAN, CA AND WECAN UNDER $\tilde{\mathcal{E}}(N = 256,\ M = 4,\ P = 50)$

	Auto-cor sidelobe peak	Cross-cor peak	$\tilde{\mathcal{E}}_{\text{norm}}$
CAN	-20.54	-18.19	0.91
CA	-21.08	-20.77	0.088
WeCAN	-31.10	-29.09	0.072

Table V compares the CA sequence and the WeCAN sequence in terms of the auto-correlation sidelobe peak (in the considered lag interval), the cross-correlation peak (in the considered lag interval) and the $\tilde{\mathcal{E}}_{\text{norm}}$ defined in (55). (The 256×4 CAN sequence is also added in Table V for comparison.) The WeCAN sequence gives the lowest correlation sidelobe peak and fitting error. Fig. 3 shows the correlation level of the CA and WeCAN sequences. We observe from Fig. 3 that the WeCAN sequence provides a "uniformly low" correlation level in the required lag interval $[1, P-1]$, while the correlation level of the CA sequence increases as the lag increases from 1 to $P-1$. This behavior is attributed to the fact that WeCAN makes use of uniform weights $\{\gamma_n = 1\}_{n=1}^{P-1}$ in (57) whereas CA implicitly assumes "uneven" weights $\{\gamma_n = P-n\}_{n=1}^{P-1}$ [see (44)], so the bigger the lag, the smaller the weight. We also note that the correlation level at $n = 0$ for the WeCAN sequence is very low [around -85 dB, although in Fig. 3(b) we limit it to -50 dB for easier comparison with Fig. 3(a)]. The reason is that we chose $\gamma_0 = 25.5$, which is much larger than the other weights (see the last paragraph) and thus the "0-lag" correlation fitting error $\|\mathbf{R}_0 - N\mathbf{I}\|$ is emphasized the most in the criterion of $\tilde{\mathcal{E}}$ in (27).

C. The Minimization of $\hat{\mathcal{E}}$ in (27)

Consider using the WeCAN algorithm to minimize the criterion $\hat{\mathcal{E}}$ in (27) with $N = 256$, $M = 4$ and the following weights:

$$\gamma_n^2 = \begin{cases} 1, & n \in [1, 19] \cup [236, 255] \\ 0, & n \in [20, 235] \end{cases} \tag{58}$$

[as before, γ_0 is chosen to ensure the positive semi-definiteness of Γ in (30)]. We still use a randomly generated sequence to initialize WeCAN. In this scenario, the normalized fitting error is defined as $\hat{\mathcal{E}}_{\text{norm}} = \hat{\mathcal{E}}/(MN^2)$.

TABLE VI
COMPARISON BETWEEN CAN AND WECAN UNDER $\hat{\mathcal{E}}(N = 256,\ M = 4)$

	Auto-cor sidelobe peak	Cross-cor peak	$\hat{\mathcal{E}}_{\text{norm}}$
CAN	-20.53	-17.68	0.40
WeCAN	-45.17	-45.81	9.54×10^{-4}

Table VI compares the WeCAN sequence and the 256×4 CAN sequence. The WeCAN sequence provides much lower correlation sidelobe peaks and much smaller fitting error. Fig. 4 shows the corresponding correlation levels of the CAN and WeCAN sequences, from which we see that WeCAN succeeds much better in suppressing the correlations at the required lags. Note that because $|r_{m_1 m_2}(N-1)| = 1$ for all m_1 and m_2, the correlation level corresponding to the maximum lag $N-1$ is always equal to $20\log_{10}(\sqrt{M^2}/\sqrt{MN^2})$, which is -42.14 dB in this case [see the end points in both Fig. 4(a) and (b)].

D. CAD Versus CA

Consider again minimizing the criterion $\tilde{\mathcal{E}}$ in (11), with $N = 256$, $M = 4$ and $P = 30$. Note that in this case $P \le (N+M)/2M$ is satisfied and therefore it is in principle possible to make $\tilde{\mathcal{E}}$ equal to zero (see the *Remark* following (18) in Section III).

We use the CA and CAD algorithms (with random initialization) to design the sequence. Fig. 5 shows the correlation levels of the CA and CAD sequences. Both of them give almost zero (-300 dB can be considered as zero in practice) correlation sidelobes in the required lag interval. The normalized fitting error $\tilde{\mathcal{E}}_{\text{norm}}$ [defined in (55)] is 3.05×10^{-24} for CA and 2.93×10^{-26} for CAD, which indicates an almost exact covariance matrix match. Thus, both the CA and CAD sequences can be considered as nearly globally-optimal in terms of minimizing the criterion $\tilde{\mathcal{E}}$. (The WeCAN algorithm is also able to give an almost zero $\tilde{\mathcal{E}}_{\text{norm}}$ in this case, but we do not show its results here for brevity.)

In all cases that we have tested, CAD and CA always performed very similarly to each other in terms of correlation level and fitting error. (For instance, if we replaced Fig. 3(a) by the plot of the CAD sequence with the same dimension, there would be little visual difference.) This fact provides empirical evidence that the "almost equivalence" between (47) and (48) holds

Authorized licensed use limited to: University of Florida. Downloaded on November 18, 2009 at 14:51 from IEEE Xplore. Restrictions apply.

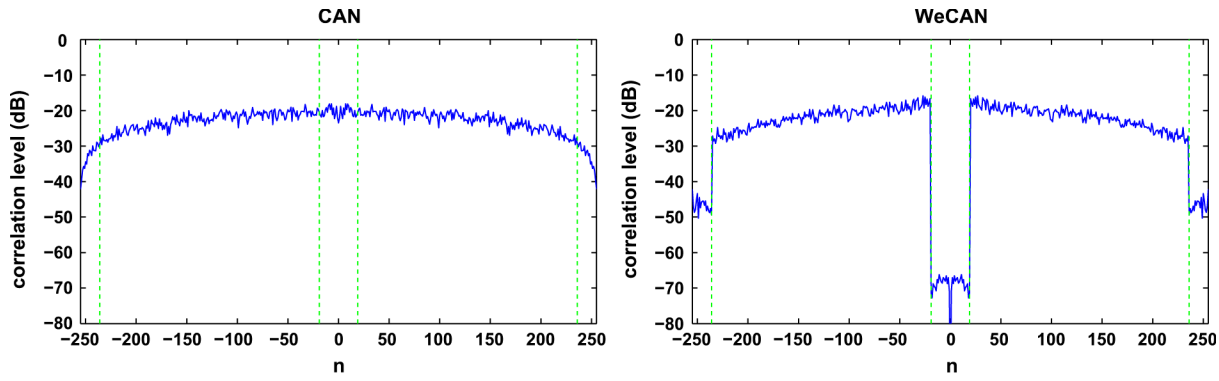

Fig. 4. Correlation levels of the CAN sequence and the WeCAN sequence for $N = 256$, $M = 4$ and weights $\{\gamma_n\}_{n=1}^{N=0}$ as specified in (58). (The dotted vertical lines signify the boundaries of the time lag interval under consideration.) (a) The CAN sequence and (b) the WeCAN sequence.

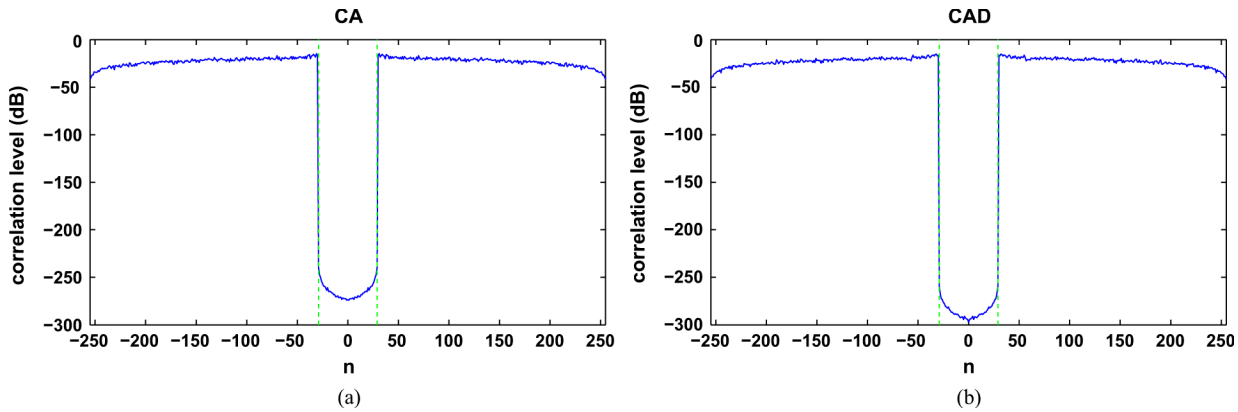

Fig. 5. Correlation levels of the CA and CAN sequence and the WeCAN sequence for $N = 256$, $M = 4$ and $P = 30$. (The dotted vertical lines signify the boundary of the time lag interval under consideration.) (a) The CA sequence and (b) the CAD sequence.

true at least from the viewpoint of algorithm performance. See Appendix B for further discussions about this aspect.

Remark: To perform well, all cyclic algorithms discussed in this paper require a proper value for the stop criterion parameter ϵ (see e.g., the last step in Table III). For the above example where the inequality $P \leq (N+M)/2M$ is satisfied, a sufficiently small ϵ (e.g., 10^{-10}) should be used to allow running enough many iterations that drive the criterion $\tilde{\mathcal{E}}$ to zero. In other examples, a "moderate" ϵ (such as 10^{-4}) is preferred to prevent the algorithm from running indefinitely without decreasing the criterion any more. ■

E. MIMO SAR Imaging Application

Consider a MIMO radar angle-range imaging example (intrapulse Doppler effects are assumed to be negligible) using uniform linear arrays with colocated $M = 4$ transmit and $M_r = 4$ receive antennas. The inter-element spacing of the transmit and receive antennas is equal to 2 and 0.5 wavelengths, respectively. Suppose that all possible targets are in a far field consisting of $P = 60$ range bins (which means that the maximum round trip delay difference within the illuminated scene is not longer than 59 subpulses) and a scanning angle area of $(-40,40)$ degrees. The length of the probing waveform for each transmit antenna is $N = 512$.

Let $\mathbf{X}$ denote the $N \times M$ transmitted probing waveform matrix [see (5)], and let

$$\tilde{\mathbf{X}} = \begin{bmatrix} \mathbf{X} \\ \mathbf{0} \end{bmatrix}_{(N+P-1)\times M} \tag{59}$$

where $\mathbf{0}$ is a $(P-1)\times M$ matrix of zeros. Then the $M_r \times (N+P-1)$ received data matrix can be written as

$$\mathbf{D}^H = \sum_{p=0}^{P-1} \sum_{k=1}^{K} \alpha_{pk} \mathbf{a}_k \mathbf{b}_k^T \tilde{\mathbf{X}}^H \mathbf{J}_p + \mathbf{E}^H \tag{60}$$

where $\mathbf{J}_p$ is an $(N+P-1)\times(N+P-1)$ shifting matrix as defined in (8) (with the same structure but different dimension), $\mathbf{E}^H$ is the noise matrix whose columns are independent and identically distributed (i.i.d.) random vectors with mean zero and covariance matrix $\mathbf{Q}$, $\{\alpha_{pk}\}_{p=1,k=1}^{P,K}$ are complex amplitudes which are proportional to the radar-cross-sections (RCS) of the scatters, and $\mathbf{a}_k$ and $\mathbf{b}_k$ are the receive and transmit steering vectors, respectively, which are given by

$$\mathbf{a}_k = [1 \quad e^{-j\pi \sin(\theta_k)} \quad \cdots \quad e^{-j\pi(M_r-1)\sin(\theta_k)}]^T \tag{61}$$

and

$$\mathbf{b}_k = [1 \quad e^{-j\pi M_r \sin(\theta_k)} \quad \cdots \quad e^{-j\pi(M-1)M_r \sin(\theta_k)}]^T \tag{62}$$

Authorized licensed use limited to: University of Florida. Downloaded on November 18, 2009 at 14:51 from IEEE Xplore. Restrictions apply.

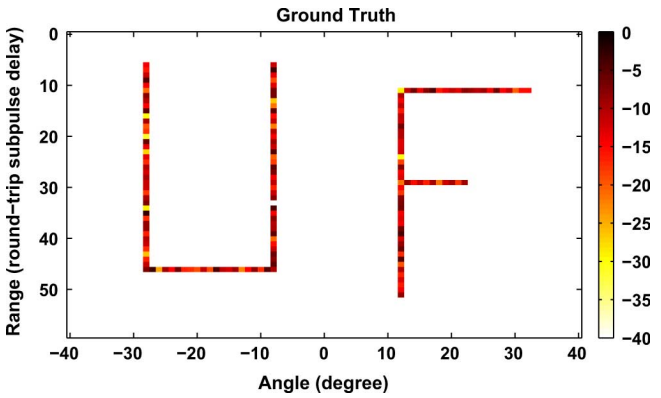

Fig. 6. True target image {the absolute of $\{\alpha_{pk}\}_{p=1,k=1}^{P,K}$ are shown).

where $\{\theta_k\}_{k=1}^{K}$ are the scanning angles. Our goal is to estimate $\{\alpha_{pk}\}_{p=1,k=1}^{P,K}$ from the collected data $\mathbf{D}^H$.

First we apply the following matched filter to the data matrix $\mathbf{D}^H$:

$$\tilde{\mathbf{X}}_p^{\mathrm{MF}} \triangleq \mathbf{J}_p^H \tilde{\mathbf{X}} (\tilde{\mathbf{X}}^H \tilde{\mathbf{X}})^{-1}, \quad (N+P-1) \times M \tag{63}$$

(note that $\tilde{\mathbf{X}}^H \mathbf{J}_p \tilde{\mathbf{X}}_p^{\mathrm{MF}} = \mathbf{I}_M$) to perform range compression for the p^{th} range bin, i.e.,

$$\begin{aligned}\tilde{\mathbf{D}}_p^H &\triangleq \mathbf{D}^H \tilde{\mathbf{X}}_p^{\mathrm{MF}} \\ &= \left(\sum_{q=0}^{P-1} \sum_{k=1}^{K} \alpha_{qk} \mathbf{a}_k \mathbf{b}_k^T \tilde{\mathbf{X}}^H \mathbf{J}_q \right) \tilde{\mathbf{X}}_p^{\mathrm{MF}} \\ &\quad + \mathbf{E}^H \tilde{\mathbf{X}}_p^{\mathrm{MF}} \\ &= \sum_{k=1}^{K} \alpha_{pk} \mathbf{a}_k \mathbf{b}_k^T \tilde{\mathbf{X}}^H \mathbf{J}_p \tilde{\mathbf{X}}_p^{\mathrm{MF}} + \mathbf{Z}_p \\ &= \sum_{k=1}^{K} \alpha_{pk} \mathbf{a}_k \tilde{\mathbf{b}}_k^H + \mathbf{Z}_p, \quad (\tilde{\mathbf{b}}_k^H \triangleq \mathbf{b}_k^T)\end{aligned} \tag{64}$$

where

$$\mathbf{Z}_p = \left(\sum_{\substack{q=0 \\ q \neq p}}^{P-1} \sum_{k=1}^{K} \alpha_{qk} \mathbf{a}_k \mathbf{b}_k^T \tilde{\mathbf{X}}^H \mathbf{J}_q \right) \tilde{\mathbf{X}}_p^{\mathrm{MF}} + \mathbf{E}^H \tilde{\mathbf{X}}_p^{\mathrm{MF}}.$$

Equation (64) leads naturally to the following least squares (LS) estimate of α_{pk}:

$$\hat{\alpha}_{pk}^{\mathrm{LS}} = \frac{\mathbf{a}_k^H \tilde{\mathbf{D}}_p^H \tilde{\mathbf{b}}_k}{\|\mathbf{a}_k\|^2 \|\tilde{\mathbf{b}}_k\|^2}, \qquad k = 1, \ldots, K \text{ and } p = 0, \ldots, P-1 \tag{65}$$

as well as to the following Capon estimate:

$$\hat{\alpha}_{pk}^{\mathrm{Capon}} = \frac{\mathbf{a}_k^H \hat{\mathbf{R}}_p^{-1} \tilde{\mathbf{D}}_p^H \tilde{\mathbf{b}}_k}{\mathbf{a}_k^H \hat{\mathbf{R}}_p^{-1} \mathbf{a}_k \|\tilde{\mathbf{b}}_k\|^2}, \qquad k = 1, \ldots, K \text{ and } p = 0, \ldots, P-1 \tag{66}$$

where $\hat{\mathbf{R}}_p = \tilde{\mathbf{D}}_p^H \tilde{\mathbf{D}}_p$ denotes the covariance matrix of the "compressed" received data (see [4] for more details about these estimates of α_{pk}).

To obtain a larger *synthetic* aperture, we use the SAR principle and thus repeat the process of "sending a probing waveform and collecting data" at $\tilde{N} = 20$ different positions; the collected data matrices are denoted as $\mathbf{D}_1^H, \mathbf{D}_2^H \ldots, \mathbf{D}_{\tilde{N}}^H$ respectively. Suppose that two adjacent positions are spaced $MM_r/2$ wavelengths apart, which induces a phase shift of $\psi_k = -2\pi MM_r/2 \sin(\theta_k)$ for both the transmit and receive steering vectors corresponding to the two adjacent positions. (As long as the "targets in the far-field" assumption holds, the distance between two adjacent positions can be chosen at will and can be different for different adjacent positions; we only need to change the phase shift ψ_k accordingly.) In this case, we let

$$\tilde{\mathbf{D}}_p^H = [\mathbf{D}_1^H \tilde{\mathbf{X}}_p^{\mathrm{MF}} \quad \mathbf{D}_2^H \tilde{\mathbf{X}}_p^{\mathrm{MF}} \quad \cdots \quad \mathbf{D}_{\tilde{N}}^H \tilde{\mathbf{X}}_p^{\mathrm{MF}}]_{M_r \times \tilde{N}M} \tag{67}$$

and

$$\tilde{\mathbf{b}}_k^H = \left[\mathbf{b}_k^T \quad \mathbf{b}_k^T e^{j2\psi_k} \quad \cdots \quad \mathbf{b}_k^T e^{j2(\tilde{N}-1)\psi_k} \right]_{1 \times \tilde{N}M}. \tag{68}$$

Using this notation, the expressions for the estimates of α_{pk} in (65) and (66) can be used *mutatis mutandis*.

In the numerical simulation, the noise covariance matrix $\mathbf{Q}$ is chosen as $\sigma^2 \mathbf{I}_{M_r}$, where $\sigma^2 = 0.001$. The targets are chosen to form a "UF" shape (see Fig. 6) and the RCS-related parameters $\{\alpha_{pk}\}_{p=1,k=1}^{P,K}$ are simulated as i.i.d. complex symmetric Gaussian random variables with mean 0 and variance 1 at the target locations and zero elsewhere. The average (transmitted) signal-to-noise ratio (SNR) is given by

$$\mathrm{SNR} = \frac{\frac{\mathrm{tr}(\mathbf{X}^H \mathbf{X})}{N}}{\mathrm{tr}(\mathbf{Q})} = \frac{M}{M_r \sigma^2} = 30 \text{ dB}. \tag{69}$$

We use two different probing sequences: the QPSK Hadamard+PN sequence and the CAD sequence with $N = 512$, $M = 4$ and $P = 60$. The transmitted waveform is phase-modulated by the probing sequence (one sequence element corresponds to one subpulse) and we assume proper sampling so that the considered discrete models are appropriate. The estimated $\{\alpha_{pk}\}_{p=1,k=1}^{P,K}$ using these two waveforms are shown in Fig. 7. The CAD waveform gives much clearer angle-range images than the Hadamard+PN waveform. Note from Fig. 7(c) and (d) that the CAD waveform facilitates almost perfect range compression via the matched filter (the false scatterers are due to the presence of noise) and that the Capon estimator provides a radar image with a high angle resolution.

VII. Concluding Remarks

In this paper we have presented several new cyclic algorithms, namely CAN, WeCAN and CAD, for the synthesis of unimodular sequence sets which can be used to phase-modulate a MIMO radar waveform. We aimed at generating sequence sets that have both good auto- and cross-correlation properties. The CAN algorithm can be used to design very long sequences (of length up to $N \sim 10^5$), which can hardly be handled by other algorithms previously suggested in the literature. The WeCAN

Authorized licensed use limited to: University of Florida. Downloaded on November 18, 2009 at 14:51 from IEEE Xplore. Restrictions apply.

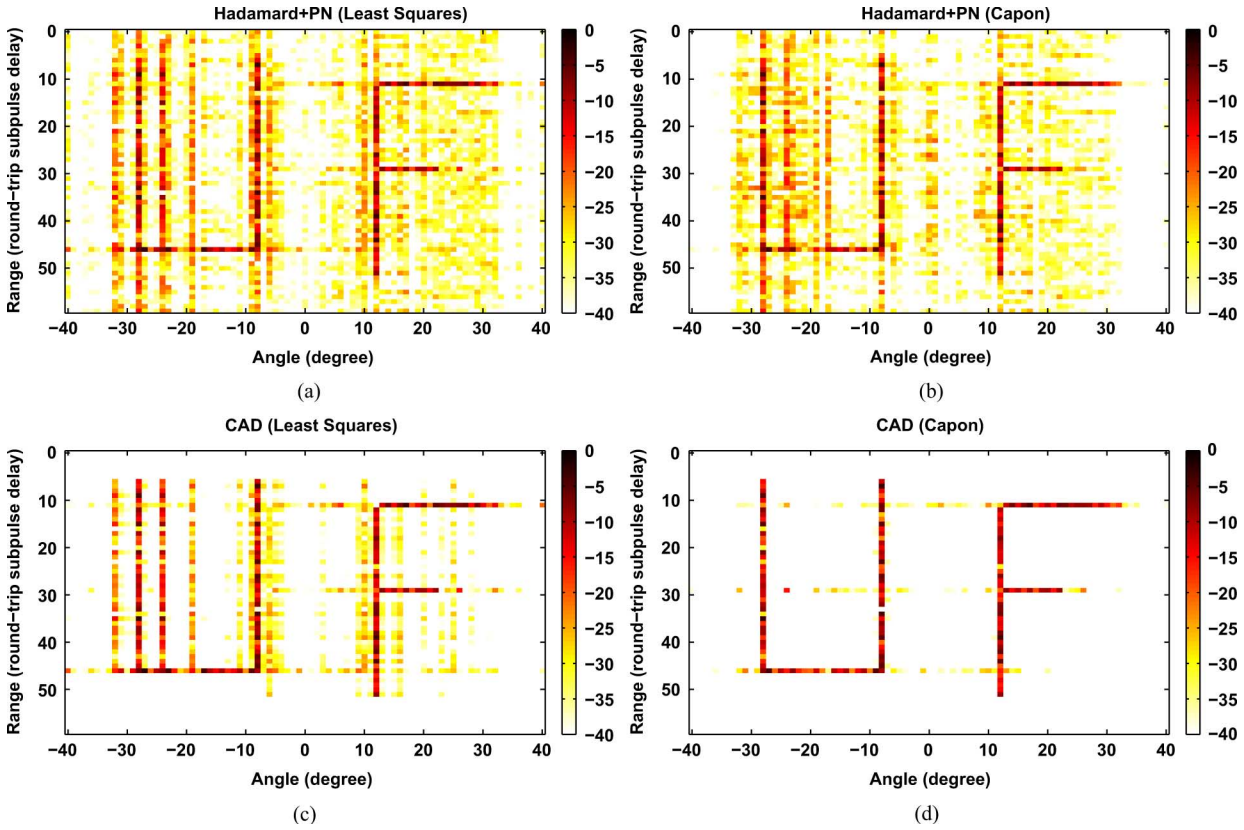

Fig. 7. Estimated target images in terms of the RCS-related parameters $\{|\alpha_{pk}|\}_{p=1,k=1}^{P,K}$. (a) The LS estimate using the Hadamard + PN waveform, (b) The Capon estimate using the Hadamard + PN waveform, (c) The LS estimate using the CAD waveform and (d) The Capon estimate using the CAD waveform.

algorithm is useful when only a few selected correlation lags are of interest. The CAD algorithm minimizes a specific form of the WeCAN criterion; unlike the other algorithms, it does so in a direct manner without relying on an "almost equivalent" criterion. The WeCAN or CAD algorithm can make the correlation levels almost zero if the lag interval of interest is sufficiently small. Several numerical examples have been presented to demonstrate the good performance of the designed sequences. The proposed sequence set design algorithms can also be used for waveform design in multiple access wireless communications applications.

Appendix A
Solving the Minimization Problem in (53)

The problem is to minimize the following single-variable function:

$$f(\phi) = -2a_1\cos(\phi+\theta_1) + a_2\cos(2\phi+\theta_2), \quad \phi\in[-\pi,\pi]. \tag{70}$$

We take the derivative of $f(\phi)$ with respect to ϕ and set it to 0:

$$f'(\phi) = 2a_1\sin(\phi+\theta_1) - 2a_2\sin(2\phi+\theta_2) = 0. \tag{71}$$

By using trigonometric identities, (71) can be written as

$$(b+d)x^4 - 2(a+2c)x^3 - 6dx^2 - 2(a-2c)x - b + d = 0,$$
$$x = \tan\left(\frac{\phi}{2}\right) \in (-\infty,\infty) \tag{72}$$

where

$$a = a_1\cos(\theta_1), \quad b = a_1\sin(\theta_1);$$
$$c = a_2\cos(\theta_2), \quad d = a_2\sin(\theta_2).$$

Equation (72) is a 4^{th}-order polynomial equation whose roots can be found in closed-form. (However, the closed-form root formula is somewhat complicated and we will actually use the companion matrix method to compute the roots, see [28]; the latter only requires computing the eigenvalues of a 4×4 matrix and works even faster than the algebraic closed-form formula.) Then we select the real-valued roots (in terms of ϕ) of (72) and form a set of these roots together with the end points $-\pi$ and π; the point in this set that gives the smallest value of $f(\phi)$ in (70) determines the minimizer ϕ of (53).

Appendix B
On "Almost Equivalence"

As mentioned in Section III, the criteria in (20) and (19) are what we can call "almost equivalent" (and so are (34) and (33) in Section IV, and (48) and (47) in Section V). For simplicity, let us assume that $M = 1$ here (in which case the designed sequence becomes $\{x(n) = e^{j\phi(n)}\}_{n=1}^{N}$). Then (19) can be written as

$$\mathcal{E} = 2N\sum_{p=1}^{2N}\left(\left|\frac{1}{\sqrt{2N}}\sum_{n=1}^{N}x(n)e^{-j\omega_p n}\right|^2 - \frac{1}{2}\right)^2. \tag{73}$$

Authorized licensed use limited to: University of Florida. Downloaded on November 18, 2009 at 14:51 from IEEE Xplore. Restrictions apply.

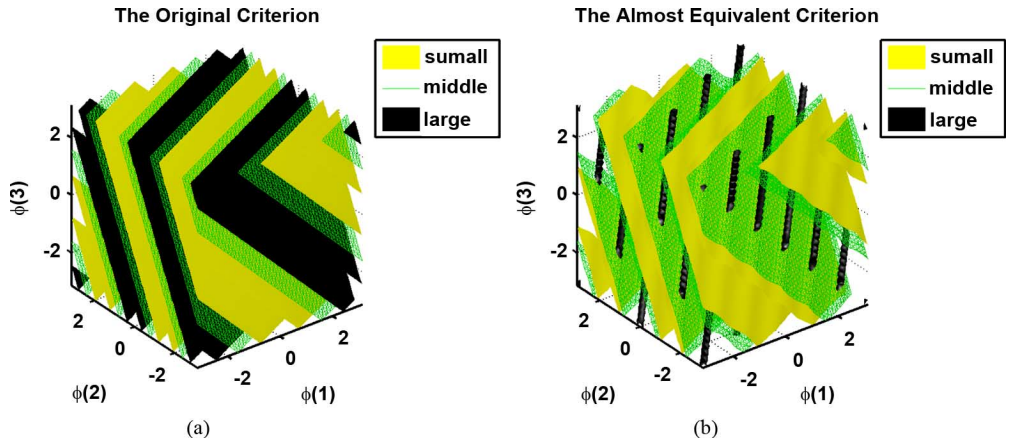

Fig. 8. The contour surface plots of the two metrics $\mathcal{E}$ and $\mathcal{E}_{\rm ae}$. Solid yellow, hatched green and solid black represent small, middle and large values, respectively. (a) The $\mathcal{E}$ in (73) and (b) $\mathcal{E}_{\rm ae}$ in (78).

Let

$$z_p = \left| \frac{1}{\sqrt{2N}} \sum_{n=1}^{N} x(n) e^{-j\omega_p n} \right|^2 \tag{74}$$

and note that $\sum_{p=1}^{2N} z_p = \sum_{n=1}^{N} |x_n|^2 = N$ (from Parseval equality). The goal is to determine $\{x(n)\}_{n=1}^{N}$ such that (73) is minimized. To simplify this determination we can first determine $\{z_p\}_{p=1}^{2N}$ such that

$$\begin{aligned} \min_{\{z_p\}_{p=1}^{2N}} \quad & \sum_{p=1}^{2N} \left(z_p - \frac{1}{2} \right)^2 \\ \text{s.t.} \quad & z_p \geq 0 \\ & \sum_{p=1}^{2N} z_p = N. \end{aligned} \tag{75}$$

That is, we over-parameterize the problem (73) via the use of $\{z_p\}_{p=1}^{2N}$ and then we will fit the right-hand-side of (74) to the so-obtained $\{\hat{z_p}\}_{p=1}^{2N}$.

The solution to (75) is obviously given by

$$\hat{z}_p = \frac{1}{2}, \quad p = 1, \ldots, 2N. \tag{76}$$

It is clear from (74) that z_p constrains the magnitude of $\sum_{n=1}^{N} x(n) e^{-j\omega_p n}$ but leaves its phase free. Therefore, fitting to $\{\hat{z_p}\}_{p=1}^{2N}$ leads to the following minimization problem:

$$\begin{aligned} \min_{\{x_n\}_{n=1}^{N}, \{\psi_p\}_{p=1}^{2N}} \quad & 2N \sum_{p=1}^{2N} \left| \frac{1}{\sqrt{2N}} \sum_{n=1}^{N} x(n) e^{-j\omega_p n} - \sqrt{\hat{z}_p} e^{j\psi_p} \right|^2 \\ \text{s.t.} \quad & |x(n)| = 1, \quad n = 1, \ldots, N \end{aligned} \tag{77}$$

which is exactly (20) for $M = 1$.

As evidenced in the foregoing analysis, the criterion in (77) is itself a correlation metric in its own right; if there exists $\{x(n)\}_{n=1}^{N}$ that makes the criterion in (77) zero, the same $\{x(n)\}_{n=1}^{N}$ will also make the original criterion in (73) zero. By continuity arguments, the $\{x(n)\}_{n=1}^{N}$ that makes (77) small will also make (73) equal to a small value.

According to the derivation in Section III [c.f. (23)], for fixed $\{x(n)\}_{n=1}^{N}$, the minimizer $e^{j\psi_p}$ is given by $\sum_{n=1}^{N} x(n) e^{-j\omega_p n} / \left| \sum_{n=1}^{N} x(n) e^{-j\omega_p n} \right|$. Thus, the criterion in (77) can be written as

$$\mathcal{E}_{\rm ae} = 2N \cdot \sum_{p=1}^{2N} \left| \frac{1}{\sqrt{2N}} \sum_{n=1}^{N} x(n) e^{-j\omega_p n} - \frac{1}{\sqrt{2}} \frac{\sum_{n=1}^{N} x(n) e^{-j\omega_p n}}{\left| \sum_{n=1}^{N} x(n) e^{-j\omega_p n} \right|} \right|^2. \tag{78}$$

To illustrate the relationship between $\mathcal{E}$ in (73) and $\mathcal{E}_{\rm ae}$ in (78), we show the contour plots of these two metrics in the case of $N = 3$. Note that both $\mathcal{E}$ and $\mathcal{E}_{\rm ae}$ are functions of the variables $\{\phi(n)\}_{n=1}^{3}$, which are the phases of $\{x(n)\}_{n=1}^{3}$ and each can take values from $-\pi$ to π. We cover the phase range $[-\pi, \pi]$ by 50 points and calculate $\mathcal{E}$ and $\mathcal{E}_{\rm ae}$ at each grid point in the three dimensional cube $[-\pi, \pi]^3$. Then we use three different colors to draw contour surfaces with values around the minimum value plus 1, the median value and the maximum value minus 1 of $\mathcal{E}$ ($\mathcal{E}_{\rm ae}$), respectively. The resulted plots are shown in Fig. 8

We can first observe from Fig. 8 that both $\mathcal{E}$ and $\mathcal{E}_{\rm ae}$ are "quite irregular" metrics with respect to $\{\phi(n)\}_{n=1}^{3}$: contour planes with different values interleave with each other and there is hardly any global direction of consistent functional increasing or decreasing. On the other hand, locally there are clear gradient structures, as seen from the sequentially repeated "yellow green black" planes, especially in Fig. 8(a). Another interesting observation is that the shape and positions of yellow and green planes (corresponding to small and middle values) in Fig. 8(a) are very similar to those of yellow and green planes in Fig. 8(b). This observation lends support to the previous claim that a sequence $\{x(n)\}_{n=1}^{3}$ resulting in a small value of $\mathcal{E}_{\rm ae}$ also makes $\mathcal{E}$ small.

In the above case where $N = 3$, we actually have

$$\begin{aligned} \mathcal{E} &= 2(|r(1)|^2 + |r(2)|^2) \\ &= 2 \left| e^{j(\phi(2) - \phi(1))} + e^{j(\phi(3) - \phi(2))} \right|^2 + 2 \geq 2. \end{aligned} \tag{79}$$

The complex sinusoidal terms in (79) imply a periodic pattern with many local minima, which can be observed from Fig. 8. Indeed, the smallest value of $\mathcal{E}$ in this example is 2.0, and it appears ten times for the $50 \times 50 \times 50$ grid points (it will appear

Authorized licensed use limited to: University of Florida. Downloaded on November 18, 2009 at 14:51 from IEEE Xplore. Restrictions apply.

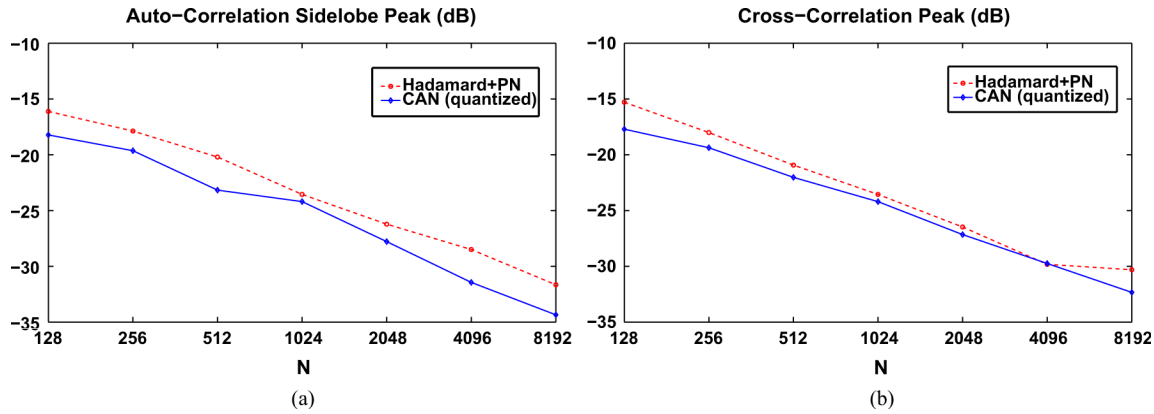

Fig. 9. Same comparisons as shown in Fig. 2(a) and (b), except that the phases of the CAN sequence used here are quantized into 32 levels.

more times if we use a finer grid). Interestingly, if we apply the CAN algorithm described in Section III, the generated sequence $\{x(n)\}_{n=1}^{3}$ makes $\mathcal{E}$ equal to 2.0 and thus achieves the global minimum. Moreover, different initial conditions (c.f. Table II) lead to different sequences, which are all global minima (i.e., making $\mathcal{E}$ equal to 2.0). This again sheds some light on the validity of the "almost equivalent" metric $\mathcal{E}_{\rm ae}$.

Appendix C
On Quantization Effect

We have assumed in this paper that the phases of the designed sequences can take on any values from $-\pi$ to π. In practice it might be required that the phases are drawn from a discrete constellation. Thus, we briefly examine here the performance of our designed sequences under quantization.

Let $\{x_m(n)\}_{m=1,n=1}^{M,N}$ denote the sequence set that is obtained from one of the algorithms discussed in this paper. Suppose that the quantization level is 2^q where $q \geq 1$ is an integer. Then the quantized sequence can be expressed as

$$\hat{x}_m(n) = \exp\left\{ j \left\lfloor \frac{\arg\{x_m(n)\}}{\frac{2\pi}{2^q}} \right\rfloor \frac{2\pi}{2^q} \right\}, \quad m = 1, \ldots, M \text{ and } n = 1, \ldots, N. \quad (80)$$

We quantize the CAN sequence used in Fig. 2 into 32 levels (i.e., $q = 5$) and do the same comparisons with the Hadamard+PN sequence. The results are shown in Fig. 9, from which we see that the curves representing the CAN sequence move up a little but they are still below the corresponding curves of the Hadamard+PN sequence [except for the point of $N = 4096$ in Fig. 9(b)]. We do not plot the fitting error here as was done in Fig. 2(c), because the fitting error of the CAN sequence almost does not change after this 32-level quantization.

Similar situations occur if we quantize sequences generated from the other algorithms (WeCAN, CAD and CA) used in Section VI. In our test, the performance degradation (i.e., the correlation sidelobe increase) was quite limited provided that the quantization level was not very small (e.g., $q \geq 6$).

References

[1] E. Fishler, A. Haimovich, R. Blum, L. Cimini, D. Chizhik, and R. Valenzuela, "Spatial diversity in radars—Models and detection performance," *IEEE Trans. Signal Process.*, vol. 54, no. 3, pp. 823–838, Mar. 2006.

[2] J. Li, P. Stoica, L. Xu, and W. Roberts, "On parameter identifiability of MIMO radar," *IEEE Signal Process. Lett.*, vol. 14, pp. 968–971, Dec. 2007.

[3] D. W. Bliss and K. W. Forsythe, "Multiple-input multiple-output (MIMO) radar and imaging: Degrees of freedom and resolution," in *Proc. 37th Asilomar Conf. Signals, Systems, Computers*, Pacific Grove, CA, Nov. 2003, vol. 1, pp. 54–59.

[4] L. Xu, J. Li, and P. Stoica, "Target detection and parameter estimation for MIMO radar systems," *IEEE Trans. Aerosp. Electron. Syst.*, vol. 44, pp. 927–939, Jul. 2008.

[5] J. Li and P. Stoica, "MIMO radar with colocated antennas: Review of some recent work," *IEEE Signal Process. Mag.*, vol. 24, no. 5, pp. 106–114, Sep. 2007.

[6] A. Haimovich, R. Blum, and L. Cimini, "MIMO radar with widely separated antennas," *IEEE Signal Process. Mag.*, vol. 25, no. 1, pp. 116–129, Jan. 2008.

[7] *MIMO Radar Signal Processing*, J. Li and P. Stoica, Eds. New York: Wiley, 2008.

[8] M. I. Skolnik, *Radar Handbook*, 2nd ed. New York: McGraw-Hill, 1990.

[9] J. Li, P. Stoica, and X. Zheng, "Signal synthesis and receiver design for MIMO radar imaging," *IEEE Trans. Signal Process.*, vol. 56, no. 8, pp. 3959–3968, Aug. 2008.

[10] J. Li, L. Xu, P. Stoica, D. Bliss, and K. Forsythe, "Range compression and waveform optimization for MIMO radar: A Cramer–Rao bound based study," *IEEE Trans. Signal Process.*, vol. 56, pp. 218–232, Jan. 2008.

[11] D. R. Fuhrmann and G. S. Antonio, "Transmit beamforming for MIMO radar systems using signal cross-correlation," *IEEE Trans. Aerosp. Electron. Syst.*, vol. 44, no. 1, pp. 1–16, Jan. 2008.

[12] P. Stoica, J. Li, and Y. Xie, "On probing signal design for MIMO radar," *IEEE Trans. Signal Process.*, vol. 55, no. 8, pp. 4151–4161, Aug. 2007.

[13] P. Stoica, J. Li, and X. Zhu, "Waveform synthesis for diversity-based transmit beampattern design," *IEEE Trans. Signal Process.*, vol. 56, no. 6, pp. 2593–2598, Jun. 2008.

[14] Y. Yang and R. S. Blum, "MIMO radar waveform design based on mutual information and minimum mean-square error estimation," *IEEE Trans. Aerosp. Electron. Syst.*, vol. 43, pp. 330–343, Jan. 2007.

[15] B. Friedlander, "Waveform design for MIMO radars," *IEEE Trans. Aerosp. Electron. Syst.*, vol. 43, pp. 1227–1238, Jul. 2007.

[16] Y. Yang and R. Blum, "Minimax robust MIMO radar waveform design," *IEEE J. Sel. Topics Signal Process.*, vol. 1, no. 1, pp. 147–155, Jun. 2007.

[17] H. Deng, "Polyphase code design for orthogonal netted radar systems," *IEEE Trans. Signal Process.*, vol. 52, no. 11, pp. 3126–3135, Nov. 2004.

[18] H. A. Khan, Y. Zhang, C. Ji, C. J. Stevens, D. J. Edwards, and D. O'Brien, "Optimizing polyphase sequences for orthogonal netted radar," *IEEE Signal Process. Lett.*, vol. 13, pp. 589–592, Oct. 2006.

[19] C.-Y. Chen and P. Vaidyanathan, "MIMO radar ambiguity properties and optimization using frequency-hopping waveforms," *IEEE Trans. Signal Process.*, vol. 56, no. 12, pp. 5926–5936, Dec. 2008.

[20] J. Oppermann and B. Vucetic, "Complex spreading sequences with a wide range of correlation properties," *IEEE Trans. Commun.*, vol. 45, pp. 365–375, Mar. 1997.

Authorized licensed use limited to: University of Florida. Downloaded on November 18, 2009 at 14:51 from IEEE Xplore. Restrictions apply.

[21] P. Stoica, H. He, and J. Li, "New algorithms for designing unimodular sequences with good correlation properties," *IEEE Trans. Signal Process.*, vol. 57, no. 4, pp. 1415–1425, Apr. 2009.
[22] H. He, P. Stoica, and J. Li, "Unimodular sequence sets with good correlations for MIMO radar," presented at the 2009 IEEE Radar Conf., Pasadena, CA, USA, May 4–8, 2009.
[23] J. A. Tropp, I. S. Dhillon, R. W. Heath, and T. Strohmer, "Designing structured tight frames via an alternating projection method," *IEEE Trans. Inf. Theory*, vol. 51, pp. 188–209, Jan. 2005.
[24] N. Levanon and E. Mozeson, *Radar Signals*. New York: Wiley, 2004.
[25] P. Stoica and R. L. Moses, *Spectral Analysis of Signals*. Upper Saddle River, NJ: Prentice-Hall, 2005.
[26] R. A. Horn and C. R. Johnson, *Matrix Analysis*. Cambridge, U.K.: Cambridge Univ. Press, 1985.
[27] D. Tse and P. Viswanath, *Fundamentals of Wireless Communication*. New York: Cambridge Univ. Press, 2005.
[28] A. Edelman and H. Murakami, "Polynomial roots from companion matrix eigenvalues," *Math. Comput.*, vol. 64, no. 210, pp. 763–776, 1995.

Hao He (S'08) received the B.Sc. degree in electrical engineering from the University of Science and Technology of China (USTC), Hefei, China, in 2007. He is currently working towards the Ph.D. degree with the Department of Electrical and Computer Engineering at the University of Florida, Gainesville.

His research interests are in the areas of spectral estimation and radar signal processing.

Petre Stoica (F'94) received the D.Sc. degree in automatic control from the Polytechnic Institute of Bucharest (BPI), Bucharest, Romania, in 1979 and an honorary doctorate degree in science from Uppsala University (UU), Uppsala, Sweden, in 1993.

He is a Professor of systems modeling with the Division of Systems and Control, the Department of Information Technology at UU. Previously, he was a Professor of system identification and signal processing with the Faculty of Automatic Control and Computers at BPI. He held longer visiting positions with Eindhoven University of Technology, Eindhoven, The Netherlands; Chalmers University of Technology, Gothenburg, Sweden (where he held a Jubilee Visiting Professorship); UU; the University of Florida, Gainesville, FL; and Stanford University, Stanford, CA. His main scientific interests are in the areas of system identification, time series analysis and prediction, statistical signal and array processing, spectral analysis, wireless communications, and radar signal processing. He has published nine books, ten book chapters, and some 500 papers in archival journals and conference records. The most recent book he coauthored, with R. Moses, is *Spectral Analysis of Signals* (Prentice-Hall, 2005).

Dr. Stoica is on the editorial boards of six journals: the *Journal of Forecasting*; *Signal Processing*; *Circuits, Signals, and Signal Processing*; *Digital Signal Processing: A Review Journal*; *Signal Processing Magazine*; and *Multidimensional Systems and Signal Processing*. He was a co-guest editor for several special issues on system identification, signal processing, spectral analysis, and radar for some of the aforementioned journals, as well as for *IEE Proceedings*. He was corecipient of the IEEE ASSP Senior Award for a paper on statistical aspects of array signal processing. He was also recipient of the Technical Achievement Award of the IEEE Signal Processing Society. In 1998, he was the recipient of a Senior Individual Grant Award of the Swedish Foundation for Strategic Research. He was also corecipient of the 1998 EURASIP Best Paper Award for Signal Processing for a work on parameter estimation of exponential signals with time-varying amplitude, a 1999 IEEE Signal Processing Society Best Paper Award for a paper on parameter and rank estimation of reduced-rank regression, a 2000 IEEE Third Millennium Medal, and the 2000 W. R. G. Baker Prize Paper Award for a paper on maximum likelihood methods for radar. He was a member of the international program committees of many topical conferences. From 1981 to 1986, he was a Director of the International Time-Series Analysis and Forecasting Society, and he was also a member of the IFAC Technical Committee on Modeling, Identification, and Signal Processing. He is also a member of the Royal Swedish Academy of Engineering Sciences, an honorary member of the Romanian Academy, and a fellow of the Royal Statistical Society.

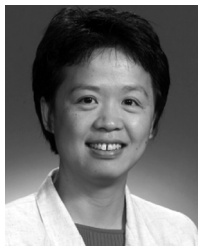

Jian Li (S'87–M'91–SM'97–F'05) received the M.Sc. and Ph.D. degrees in electrical engineering from Ohio State University, Columbus, in 1987 and 1991, respectively.

From April 1991 to June 1991, she was an Adjunct Assistant Professor with the Department of Electrical Engineering, Ohio State University, Columbus. From July 1991 to June 1993, she was an Assistant Professor with the Department of Electrical Engineering, University of Kentucky, Lexington. Since August 1993, she has been with the Department of Electrical and Computer Engineering, University of Florida, Gainesville, where she is currently a Professor. In fall 2007, she was on sabbatical leave at MIT, Cambridge, Massachusetts. Her current research interests include spectral estimation, statistical and array signal processing, and their applications.

Dr. Li is a Fellow of IET. She is a member of Sigma Xi and Phi Kappa Phi. She received the 1994 National Science Foundation Young Investigator Award and the 1996 Office of Naval Research Young Investigator Award. She was an Executive Committee Member of the 2002 International Conference on Acoustics, Speech, and Signal Processing, Orlando, FL, May 2002. She was an Associate Editor of the IEEE TRANSACTIONS ON SIGNAL PROCESSING from 1999 to 2005, an Associate Editor of the *IEEE Signal Processing Magazine* from 2003 to 2005, and a member of the Editorial Board of *Signal Processing*, a publication of the European Association for Signal Processing (EURASIP), from 2005 to 2007. She has been a member of the Editorial Board of *Digital Signal Processing—A Review Journal*, a publication of Elsevier, since 2006. She is presently a member of the Sensor Array and Multichannel (SAM) Technical Committee of the IEEE Signal Processing Society. She is a coauthor of the papers that have received the First and Second Place Best Student Paper Awards, respectively, at the 2005 and 2007 Annual Asilomar Conferences on Signals, Systems, and Computers in Pacific Grove, CA. She is also a coauthor of the paper that has received the M. Barry Carlton Award for the best paper published in the IEEE TRANSACTIONS ON AEROSPACE AND ELECTRONIC SYSTEMS in 2005.

Authorized licensed use limited to: University of Florida. Downloaded on November 18, 2009 at 14:51 from IEEE Xplore. Restrictions apply.